Self-organization of fermionic atoms in a dissipative cavity

Jeannette Alicja De Marco

Masterarbeit in Physik
angefertigt im Physikalischen Institut

vorgelegt der
Mathematisch-Naturwissenschaftlichen Fakultät
der
Rheinischen Friedrich-Wilhelms-Universität
Bonn

Dezember 2021

I hereby declare that this thesis was formulated by myself and that no sources or tools other than those cited were used.

Bonn, ...
Date Signature

1. Gutachterin: Prof. Dr. Corinna Kollath
2. Gutachter: Prof. Dr. Sebastian Diehl

Acknowledgements

First of all I would like to thank Prof. Dr. Corinna Kollath for giving me the opportunity of writing my master thesis in her research group. I was very pleased to rejoin the group after also writing my bachelor thesis here. Thanks for supporting me in all matters! I would also like to thank Prof. Dr. Sebastian Diehl for being the second referee for this thesis.

Furthermore, I would like to thank Dr. Catalin-Mihai Halati, Dr. Ameneh Sheikhan and Luisa Tolle for their help and support during the whole project. I could learn a lot from you and it was always fun to discuss. I am also very grateful to Prof. Dr. Andreas Läuchli for providing an exact diagonalization code that made part of this work possible in the first place. Moreover, I would like to thank Dr. Oliver Freyermuth for his support regarding my IT problems. I further acknowledge the generous support of the Bonn-Cologne Graduate School Honors Branch during my studies.

Finally, I would like to thank my family and friends especially Kilian Bönisch for always believing in me.

Contents

1 Introduction

In recent years, the research field of light-matter interaction has grown rapidly. Outstanding progress in the field of ultracold atomic gases has made this possible, as they provide an extremely well-controlled and tunable environment for simulating quantum systems [1]. The coupling of these ultracold atomic gases to optical cavity modes has led to interesting and novel phenomena due to various competing energy scales. In particular, atomic short-range interactions compete with cavity induced long-range interactions leading to rich phase diagrams. This was already highlighted in one of the early experiments performed in the research group of Tilman Esslinger [2], where a transversely driven Bose-Einstein condensate inside an optical cavity showed a quantum phase transition into a self-organized state. Since then, it was aimed for generalizations of these systems. By using optical lattices for the confinement of the atoms, a variety of Hubbard models with cavity-mediated long-range interactions were realized. One example for this is an extended Bose-Hubbard model with long-range interactions. Its experimentally studied phase diagram showed besides a superfluid and Mott insulating phase additionally a charge density wave and a supersolid phase [3]. However, this is still experimentally challenging for fermionic atoms. Recently, the superradiant phase transition was observed for a Fermi gas inside an optical cavity [4] but the confinement of the atoms still has to be realized in the future.

In general, ultracold atoms which are globally coupled to optical cavities are a paradigmatic example for an open quantum system. However, the openness of the systems makes it theoretically even more challenging to describe them [5]. Often, a mean-field decoupling of the cavity field and the atoms followed by an adiabatic elimination of the cavity field is used [6–8]. Trying to find theoretical methods which go beyond this mean-field approach is hence of great interest. In the research group of Corinna Kollath and Achim Rosch, analytical and numerical methods were developed for a bosonic system considering effects of fluctuations beyond the mean-field level [9–13]. In this thesis, we want to apply part of the analytical methods on an analogous model for fermionic atoms in order to investigate the self-organization phase transition.

We study a chain of (interacting) fermions globally coupled to a dissipative cavity mode. First we introduce the framework of Markovian open quantum systems in Chapter 2 and then we give a brief derivation of the theoretical model in Chapter 3. In Chapter 4, we perform a mean-field decoupling between the atoms and the cavity field which sets the basis for the description of the self-organization transition. We go beyond this approach by capturing the effect of fluctuations using a many-body adiabatic elimination method presented in the same chapter. Since thermalization plays a crucial role for the applicability of a thermal ansatz used within the many-body adiabatic elimination, we investigate the level statistics of the atomic part of our Hamiltonian in Chapter 5, which is essentially given by the ionic Hubbard model. Showing the non-integrability of this model then justifies our ansatz.

With this theoretical tools at hand, we can then start the discussion of the self-organization transition in Chapter 6 in the non-interacting limit of the model. There, we introduce the concept of symmetries in open quantum systems since this model has a so-called strong symmetry leading to multiple steady state solutions in the system. Thus, we study the self-organization transition for each of these solutions and discuss emerging differences. In Chapter 7, we investigate the interacting model by focusing on the differences in the resulting phase transitions of the mean-field approach with and without fluctuations. We find significant deviations in particular in the nature of the atomic state showing the essential influence of fluctuations onto our system. Additionally, we again find strong symmetries present in this interacting model and discuss the influence of the symmetries onto the self-organization transition.

2 Theory of open quantum systems

As the starting point for our theoretical description of ultracold atoms coupled to a dissipative cavity mode, we give a short introduction to open quantum systems and an overview on the derivation of the Lindblad master equation. For this, we follow Breuer and Petruccione [5].

An open quantum mechanical system S is a system which is in contact with an environment E. Both systems have their own Hilbert spaces $\mathcal{H}_S$ and $\mathcal{H}_E$ which give the Hilbert space of the complete system

$$\mathcal{H} = \mathcal{H}_S \otimes \mathcal{H}_E. \tag{2.1}$$

Analogously, the Hamiltonian for the total system can be decomposed out of the Hamiltonians of the system S and the environment E as

$$H = H_S \otimes \mathbb{1}_E + \mathbb{1}_S \otimes H_E + H_{SE}. \tag{2.2}$$

The additional Hamiltonian H_{SE} describes the interaction between the two systems. Usually, it is not feasible to study the full system because of the huge amount of degrees of freedom of the environment. But under certain assumptions, one can capture the effective dynamics of the open system S under the action of the environment E. In the following, we want to give a brief overview on that.

We start by looking at the full system which is described by a density matrix ρ. The dynamics of the density matrix are determined by the Liouville- von Neumann equation

$$\frac{\partial}{\partial t}\rho = -\frac{i}{\hbar}[H, \rho]. \tag{2.3}$$

By performing the partial trace over the Hilbert space of the environment, we can define the reduced density matrix of the system S as $\rho_S = \mathrm{Tr}_E(\rho)$. Similarly, we define the reduced density matrix of the environment as $\rho_E = \mathrm{Tr}_S(\rho)$ by performing the partial trace over the Hilbert space of S. With this definition and Eq. (2.3) we find that the reduced density matrix of the system S is given by

$$\rho_S(t) = \mathrm{Tr}_E[U(t, t_0)\rho(t_0)U(t, t_0)^\dagger], \tag{2.4}$$

where U is the unitary time-evolution operator of the full system. Again, in most situations, it is not feasible to calculate the full evolution. Hence, we would like to first trace out the environment and then perform the time evolution only for the reduced density matrix of S. For this, we first make the assumption that initially at $t = t_0$ the system and the environment are decoupled from each other and that the environment remains constant in time

$$\rho(t_0) = \rho_S(t_0) \otimes \rho_E. \tag{2.5}$$

This is valid if the environment is large enough so that it will not be significantly effected by the dynamics of S. Further, we assume that the evolution of the system S is Markovian. This means that the future time evolution of this system only depends on its current state, i.e. the past trajectory of the system S has no influence on the future time evolution. This is true if the relaxation time scales of the environment are much shorter than the time scales of the system-environment coupling. For systems in the field of quantum optics and ultracold atoms, the Markov property is usually well-fulfilled, but note that in general this has to be checked carefully. Under those assumptions, one finds the quantum master equation in Lindblad form

$$\frac{\partial}{\partial t}\rho_S = \mathcal{L}(\rho_S) = -\frac{i}{\hbar}[H_S, \rho_S] + \mathcal{D}(\rho_S) \tag{2.6}$$

with

$$\mathcal{D}(\rho_S) = \frac{1}{2}\sum_i \gamma_i \cdot (2L_i\rho_S L_i^\dagger - L_i^\dagger L_i \rho_S - \rho_S L_i^\dagger L_i). \tag{2.7}$$

Here, the Lindbladian $\mathcal{L}$ generates the Markovian time evolution and contains the dissipator $\mathcal{D}(\rho_S)$ with certain Lindblad or jump operators L. This models the effect of the environment on the system S with coupling strengths γ_i. Without the dissipator, the time evolution would be given by $\rho_S(t) = U_S(t,t_0)\rho_S(t_0)U_S(t,t_0)^\dagger$ with U_S corresponding to a unitary time evolution on $\mathcal{H}_S$. This unitarity is broken by the dissipator. Note that the Lindblad equation preserves the hermiticity, the trace, and the positive semidefiniteness of the density matrix.

3 Fermi-Hubbard chain coupled to a dissipative cavity mode

The system which we want to study in this thesis consists of interacting ultracold fermionic atoms which are confined to a one-dimensional optical lattice. The atoms are coupled to the field of a dissipative cavity mode and are driven by a transverse laser beam.

Following Maschler, Mekhov, and Ritsch [6] and Mivehvara et al. [8], we start the derivation of our theoretical model by describing N two-level atoms with internal states $\{|g\rangle, |e\rangle\}$, mass m and transition frequency ω_{eg}. These atoms are strongly interacting with a single standing wave cavity mode of frequency ω_c and are coherently driven by a transverse pump beam at frequency ω_p. In the rotating frame of the pump beam, this system can be described by the many-body Hamiltonian

$$H = H_\mathrm{a} + H_\mathrm{c} + H_\mathrm{ac} + H_\mathrm{ap}, \tag{3.1}$$

where the different parts will by analyzed in the following.

The atomic Hamiltonian H_a is given by

$$\begin{aligned} H_\mathrm{a} = \int \mathrm{d}^3x \left[\Psi_g^\dagger(\mathbf{x})\left(-\frac{\hbar^2}{2m}\nabla^2 + V_g(\mathbf{x})\right)\Psi_g(\mathbf{x}) + \Psi_e^\dagger(\mathbf{x})\left(-\frac{\hbar^2}{2m}\nabla^2 + V_e(\mathbf{x}) - \hbar\delta_\mathrm{a}\right)\Psi_e(\mathbf{x})\right] \\ + \frac{1}{2}\sum_{\tau,\tau'=g,e} g_{\tau\tau'}\int \mathrm{d}^3x\, \Psi_{\tau'}^\dagger(\mathbf{x})\Psi_\tau^\dagger(\mathbf{x})\Psi_\tau(\mathbf{x})\Psi_{\tau'}(\mathbf{x}) \end{aligned} \tag{3.2}$$

with the atomic field operators $\Psi_g(\mathbf{x})$ and $\Psi_e(\mathbf{x})$ for annihiating an atom at position $\mathbf{x}$ in the ground state and the excited state, respectively. V_g and V_e are external trapping potentials for the atoms. The detuning of the atomic transition frequency from the pump field frequency is given by $\delta_\mathrm{a} = \omega_p - \omega_{eg}$. The second line describes the two-body interaction with g_{gg}, g_{ee} and $g_{eg} = g_{ge}$ being related to the s-wave scattering lengths $a_{\tau\tau'}$ by $g_{\tau\tau'} = 4\pi a_{\tau\tau'}\hbar^2/m$.

The cavity field is described as a harmonic oscillator with associated Hamiltonian

$$H_\mathrm{c} = \hbar\delta_\mathrm{c} a^\dagger a, \tag{3.3}$$

where the detuning of the cavity frequency from the pump field frequency is denoted by $\delta_\mathrm{c} = \omega_\mathrm{c} - \omega_\mathrm{p}$.

The coupling between the atoms and the cavity field reads

$$H_\mathrm{ac} = -i\hbar\int \mathrm{d}^3x \left[\Psi_g^\dagger(\mathbf{x})g(\mathbf{x})a^\dagger\Psi_e(\mathbf{x}) - \Psi_e^\dagger(\mathbf{x})g(\mathbf{x})a\Psi_g(\mathbf{x})\right] \tag{3.4}$$

with the cavity mode function g and the interaction between the atoms and the pump laser beam is given by

$$H_\mathrm{ap} = -i\hbar\int \mathrm{d}^3x \left[\Psi_g^\dagger(\mathbf{x})h(\mathbf{x})\Psi_e(\mathbf{x}) - \Psi_e^\dagger(\mathbf{x})h(\mathbf{x})\Psi_g(\mathbf{x})\right], \tag{3.5}$$

where the mode function of the transverse pump field is represented by h.

In order to describe the dynamics of this system, one can look at the Heisenberg equations of motion for the atomic and photonic field operators. As we are interested in regimes with temperatures close to $T = 0$, heating processes such as spontaneous emission have to be avoided. Therefore, the pump frequency is assumed to be far detuned from the atomic transition frequency such that there is only weak atomic excitation. The shortest time scale in the system is then $1/|\delta_\mathrm{a}|$. In this limit, the excited states can be adiabatically eliminated from the dynamics by approximating

$$\Psi_e(\mathbf{x}) = -\frac{i}{\delta_\mathrm{a}}(g(\mathbf{x})a + h(\mathbf{x}))\Psi_g(\mathbf{x}). \tag{3.6}$$

Inserting this expression in the equations of motion for $\Psi_g(\mathbf{x})$ and a, one can find an effective Hamiltonian capturing the dynamics of the system in our limit

$$\begin{aligned} H_{\text{eff}} = &\int \mathrm{d}^3x\, \Psi_g^\dagger(\mathbf{x}) \left\{ -\frac{\hbar^2}{2m}\nabla^2 + V_g(\mathbf{x}) + \frac{\hbar}{\delta_{\text{a}}}(h^2(\mathbf{x}) + g^2(\mathbf{x})a^\dagger a + h(\mathbf{x})g(\mathbf{x})(a+a^\dagger)) \right\} \Psi_g(\mathbf{x}) \\ &+ \frac{g_{gg}}{2}\int \mathrm{d}^3x\, \Psi_g^\dagger(\mathbf{x})\Psi_g^\dagger(\mathbf{x})\Psi_g(\mathbf{x})\Psi_g(\mathbf{x}) + \hbar\delta_{\text{c}} a^\dagger a. \end{aligned} \tag{3.7}$$

By using optical lattices, one can reduce the dimensionality of the system to a one-dimensional chain along the cavity axis. The corresponding mode function of the cavity is given by $g(x) = g_0\cos(kx)$ with the cavity wavevector k. Because of the fact that the transverse pump beam is a broad standing wave, which is perpendicular to the cavity axis, it is constant for all sites of the lattice. Hence, $h(x) = h_0\cos(k_p y)$ with the pump wavevector k_p. Furthermore, the trapping potential along the cavity axis is given by $V_g(x) = V_0\cos(kx)^2$.

Finally, we expand the atomic field operator $\Psi_g(x)$ in terms of single atom Wannier functions ω_n as

$$\Psi_g(x) = \sum_n \sum_i c_{n,i}\, \omega_n(x - x_i), \tag{3.8}$$

where $c_{n,i}$ corresponds to the annihilation of a fermion in the n-th energy band at site i. Assuming that the involved energies are much smaller than the excitation energies between the lowest band and the second lowest band, we can restrict the Wannier expansion to the lowest energy band. We then end up with the Hamiltonian[1]

$$H = H_{\text{cav}} + H_{\text{kin}} + H_{\text{int}} + H_{\text{ac}} \tag{3.9}$$

where now

$$\begin{aligned} H_{\text{cav}} &= \hbar\delta a^\dagger a \\ H_{\text{kin}} &= -J\sum_{j=1}^{L}\sum_{\sigma\in\{\uparrow,\downarrow\}} (c_{j,\sigma}^\dagger c_{j+1,\sigma} + c_{j+1,\sigma}^\dagger c_{j,\sigma}) \\ H_{\text{int}} &= U\sum_{j=1}^{L} n_{j,\uparrow}n_{j,\downarrow} \\ H_{\text{ac}} &= -\hbar\Omega(a+a^\dagger)O \quad \text{with} \quad O = \sum_{j=1}^{L}\sum_{\sigma\in\{\uparrow,\downarrow\}} (-1)^j n_{j,\sigma}. \end{aligned} \tag{3.10}$$

Here, $n_{j,\sigma} = c_{j,\sigma}^\dagger c_{j,\sigma}$, N is the total number of fermionic atoms and L stands for the number of sites of the chain. H_{kin} describes the tunneling process of the atoms with amplitude J and H_{int} includes the repulsive onsite interaction of the atoms of strength U. The coupling between the cavity field and the total imbalance between the odd and even sites of the chain is represented by H_{ac} with amplitude Ω. This imbalance is due to the periodicity of the cavity mode which has twice the periodicity of the lattice spacing within the chain.

In order to capture the dissipative nature of the cavity, we use the Lindblad Master equation

$$\frac{\partial}{\partial t}\rho = -\frac{i}{\hbar}[H,\rho] + \frac{\Gamma}{2}\left(2a\rho a^\dagger - a^\dagger a\rho - \rho a^\dagger a\right), \tag{3.11}$$

which was introduced in the previous chapter. The jump operator is the photonic annihilation operator a which induces the decay of the cavity field through the cavity mirrors with strength Γ. Since photon losses take place fast compared to the time scale of the evolution of the system, the assumption of Markovianity is valid. Hence, the Lindblad equation is well-suited for our purpose. The presented model has a lot of interesting symmetries, which we want to investigate throughout this thesis. One of them is the $\mathbb{Z}_2$ symmetry related to the inversion of the sign of the cavity field

[1] Note that the spin degree of freedom was added into the Hamiltonian. For more details, we refer to Mivehvara et al. [8].

a and the atomic odd-even imbalance O. Since this transformation does not commute with the jump operator a of the Lindblad equation, it is only a weak symmetry meaning that it does not necessarily lead to conserved quantities. The concept of symmetries of open quantum systems will be discussed in more detail in Sec. 6.2. The complete model is sketched in Fig. 3.1.

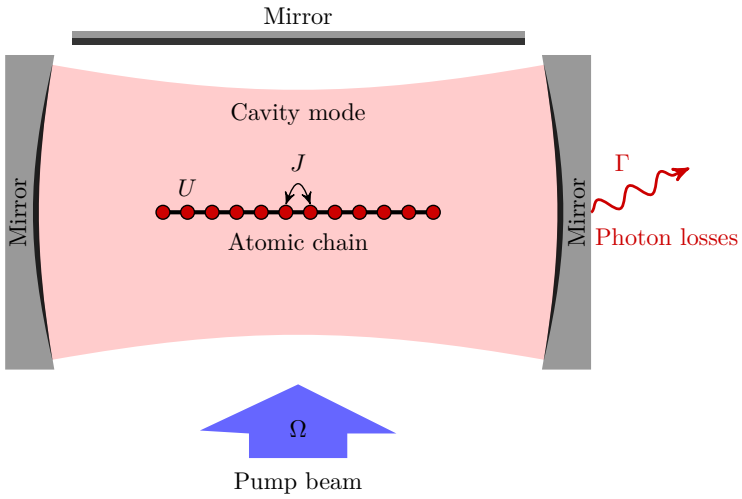

Figure 3.1: Illustration of the fermionic chain inside a single-mode cavity driven by a transverse laser beam with amplitude Ω. The atoms can tunnel to the nearest neighbour sites with amplitude J and have on-site interaction of strength U. The loss rate of the cavity is captured by Γ. Due to the periodicity of the cavity mode, which has twice the periodicity of the lattice spacing within the chain, the cavity field is coupled to the total imbalance between the odd and even sites of the chain.

4 Methods

In this chapter, we first introduce a mean-field approach in order to find the steady state solutions of the model described previously. Secondly, we present the many-body adiabatic elimination method which we use in order to go beyond the mean-field approach by taking the fluctuations of the latter into account.

4.1 Mean-field decoupling of H_{ac}

Following Halati [13], we start by performing a mean-field decoupling of H_{ac} by rewriting the coupling between the subsystems in terms of the mean-fields $\Delta := \langle O \rangle_{\mathrm{a}}$ and $\lambda := \langle a + a^\dagger \rangle_{\mathrm{c}}$, i.e.

$$(a+a^\dagger)O = (a+a^\dagger)\langle O\rangle_{\mathrm{a}} + O\langle a+a^\dagger\rangle_{\mathrm{c}} + \underbrace{(O-\langle O\rangle_{\mathrm{a}})}_{\delta O}\underbrace{(a+a^\dagger-\langle a+a^\dagger\rangle_{\mathrm{c}})}_{\delta(a+a^\dagger)} - \underbrace{\langle a+a^\dagger\rangle_{\mathrm{c}}\langle O\rangle_{\mathrm{a}}}_{\text{const.}}, \quad (4.1)$$

where the averages $\langle\cdot\rangle_{\mathrm{a}}$ and $\langle\cdot\rangle_{\mathrm{c}}$ are taken with respect to the atomic and cavity mode density matrices, respectively. Using this we find

$$H_{\mathrm{ac}} = H_{\mathrm{ac}}^{\mathrm{MF}} + \delta H_{\mathrm{ac}} + \text{const.}, \quad (4.2)$$

with

$$\begin{aligned} H_{\mathrm{ac}}^{\mathrm{MF}} &= -\hbar\Omega(a+a^\dagger)\Delta - \hbar\Omega\lambda O, \\ \delta H_{\mathrm{ac}} &= -\hbar\Omega(a+a^\dagger-\lambda)(O-\Delta), \end{aligned} \quad (4.3)$$

where $H_{\mathrm{ac}}^{\mathrm{MF}}$ gives us the mean-field contribution to the resulting Hamiltonian as it describes the influence of the atomic system onto the cavity and vice versa. δH_{ac} describes the fluctuations from the mean-field values, which we are going to include within the many-body elimination method in the next section. The constant term only leads to a shift of the energy and will drop out anyway. With this, we can now define the following decoupled mean-field Hamiltonians

$$\begin{aligned} H_{\mathrm{a}}(\lambda) &= H_{\mathrm{kin}} + H_{\mathrm{int}} - \hbar\Omega\lambda O, \\ H_{\mathrm{c}}(\Delta) &= H_{\mathrm{cav}} - \hbar\Omega(a+a^\dagger)\Delta. \end{aligned} \quad (4.4)$$

In order to find a relation between the two mean-fields, we consider the Heisenberg equation of motion for the cavity field. The Lindblad master equation gives the equation of motion for an operator A as

$$\frac{\partial}{\partial t}A = \frac{i}{\hbar}[H,A] + \frac{1}{2}\sum_i \gamma_i \cdot (2L_i A L_i^\dagger - L_i^\dagger L_i A - A L_i^\dagger L_i) \quad (4.5)$$

[5]. For the expectation value of the cavity operator a, this gives

$$i\hbar\frac{\partial}{\partial t}\langle a\rangle = -\Omega\langle O\rangle + (\delta - i\Gamma/2)\langle a\rangle. \quad (4.6)$$

Assuming that the dynamics of the cavity field are fast, we only consider the steady state of this equation resulting in

$$\alpha = \langle a\rangle = \frac{\Omega}{\delta - i\Gamma/2}\langle O\rangle \quad (4.7)$$

which relates the expectation value of the cavity field with the expectation value of the odd-even imbalance. It is straight forward to check that in this steady state limit, the cavity is in a coherent state. Using this relation, we can find the effective Hamiltonian for the atoms

$$H_{\mathrm{eff}} = H_{\mathrm{kin}} + H_{\mathrm{int}} - \hbar\Omega(\alpha+\alpha^*)O, \quad (4.8)$$

which has to be determined self-consistently as α depends on the odd-even imbalance.

Before we use this as a starting point for the next treatment, we want to have a look at the solution of this effective model. For this, we assume that the atoms are in the ground state of the effective model which we determine by exactly diagonalizing the effective Hamiltonian. The solution for the steady state is a pure state consisting of a tensor product between states of the atomic and photonic sector

$$\rho^{\mathrm{MF}} = |\alpha(\Delta_{\mathrm{eff}}), \Delta_{\mathrm{eff}}\rangle \langle \alpha(\Delta_{\mathrm{eff}}), \Delta_{\mathrm{eff}}| \,, \tag{4.9}$$

where Δ_{eff} is the effective imbalance defined as the expectation value of the odd-even imbalance in the ground state of the effective Hamiltonian. The cavity is in a coherent state $|\alpha(\Delta_{\mathrm{eff}})\rangle$ and the atoms are in the ground state $|\Delta_{\mathrm{eff}}\rangle$ of H_{eff} where $\alpha(\Delta_{\mathrm{eff}})$ and Δ_{eff} fulfill the self-consistency condition. Within the mean-field approach the self-organization transition is visible above a certain threshold of the coupling strength Ω. Then the cavity field takes a finite value and the atoms self-organize into a density modulated pattern either on the odd or even sites of the chain. This spontaneously breaks the $\mathbb{Z}_2$ symmetry. The sudden occupation of the cavity can be seen in Fig. 4.1.

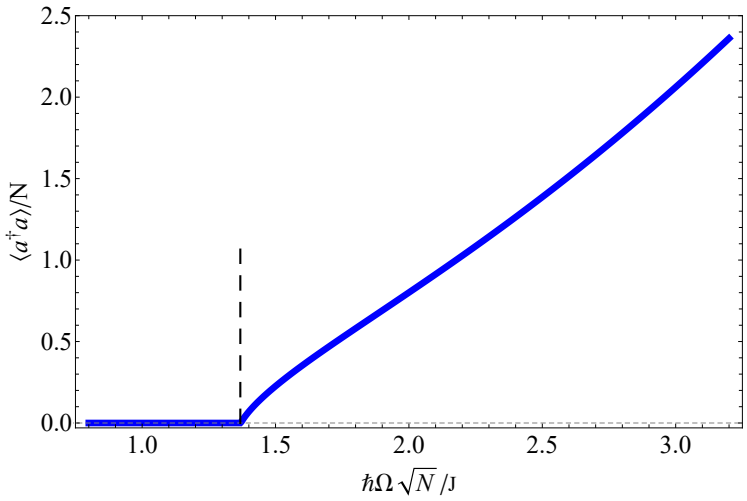

Figure 4.1: Dependence of the mean-field value of the scaled photon number $\langle a^\dagger a\rangle/N$ on the coupling strength $\hbar\Omega\sqrt{N}/J$ for $N/L = 1/2$. The parameters are $\hbar\delta/J = 2$, $U/J = 2$ and $\hbar\Gamma/J = 1$. The critical value of the self-organization transition is marked by the dashed vertical line.

4.2 Many-body adiabatic elimination

The many-body adiabatic elimination method is a perturbation theory for density matrices. It captures the effective dynamics of the density matrix in the decoherence free subspace, which is spanned by the states of the unperturbed system which do not decay under the dissipation. This approach is valid for long times because of the exponential decay of the contributions to the density matrix from the other subspaces. Hence, by using this method, we can study the behavior of our system close to the steady state. Here, we follow Sciolla, Poletti, and Kollath [14].

4.2.1 Derivation of the effective equation of motion

We start by giving a short overview of the derivation of the effective equation of motion for the density matrix in the decoherence free subspace. For this, we consider a general Lindblad equation given by

$$\frac{\partial}{\partial t}\rho = \mathcal{L}(\rho) = -\frac{i}{\hbar}\left[H_0 + H_\nu, \rho\right] + \frac{\Gamma}{2}\sum_m \left(2K_m\rho K_m^\dagger - K_m^\dagger K_m\rho - \rho K_m^\dagger K_m\right) \tag{4.10}$$

with the jump operators K_m and the dissipation strength Γ. We assume that the Hamiltonian has two contributions H_0 and H_ν, where H_ν is weak and we define $\mathcal{V}(\rho) = -\frac{i}{\hbar}[H_\nu, \rho]$ as our perturbation. Further, we can compute the eigenvalues and eigenstates of $\mathcal{L}_0 = \frac{i}{\hbar}[H_0, \cdot]$, i.e.

$$\mathcal{L}_0 \rho_\lambda = (-\lambda^R + i\lambda^I)\rho_\lambda, \tag{4.11}$$

where $\lambda^R \geq 0$ and λ^I are real numbers. For a large enough dissipation strength, λ^R either vanishes or lies in bands separated by gaps of order $O(\gamma)$, where only H_ν couples states of the different bands. We define Λ_α as the subspace of right eigenvectors with the same λ^R_α. Besides, we call Λ_0 the decoherence free subspace for which $\lambda^R_0 = 0$ holds. For the other higher subspaces $\Lambda_{\alpha\neq 0}$, one gets an exponential decay of the states in time at a rate $O(\gamma)$. Hence, the dynamics is dominated by an effective one in the decoherence free subspace for times $t \gg \gamma^{-1}$. A schematic illustration of the spectrum of the Liouvillian $\mathcal{L}_0$ can be seen in Fig. 4.2.

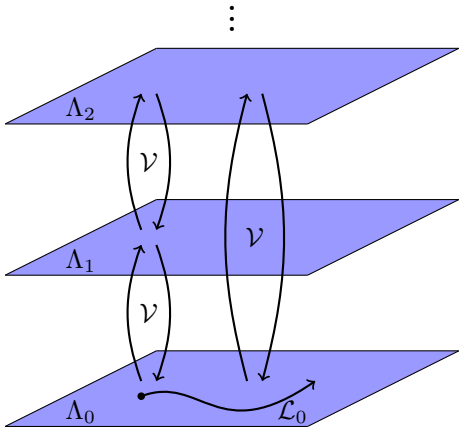

Figure 4.2: Schematic illustration of the spectrum of the Liouvillian $\mathcal{L}_0$. The eigenstates of $\mathcal{L}_0$ which have eigenvalues with the same real part span the different subspaces Λ_α. The decoherence free subspace Λ_0 contains only states whose real part of the eigenvalues vanishes. $\mathcal{L}_0$ gives the evolution within a subspace whereas $\mathcal{V}$ can induce transitions between the different subspaces Λ_α.

By adiabatically eliminating the decaying subspaces $\Lambda_{\alpha\neq 0}$, one finds an equation describing the effective dynamics with an effective Lindbladian $\tilde{\mathcal{L}}^{\Lambda_0}$

$$\begin{aligned} \frac{\partial}{\partial t}\rho^{\Lambda_0} &= \tilde{\mathcal{L}}^{\Lambda_0}\left(\rho^{\Lambda_0}\right), \\ \tilde{\mathcal{L}}^{\Lambda_0} &= \mathcal{L}_0^{\Lambda_0} - \sum_{\alpha\neq 0} \mathcal{V}^{\Lambda_0\Lambda_\alpha}\left(\mathcal{L}_0^{\Lambda_\alpha}\right)^{-1}\mathcal{V}^{\Lambda_\alpha\Lambda_0}. \end{aligned} \tag{4.12}$$

Here, the projection of the density matrix to a subspace X was defined by $\rho^X = P_X(\rho)$ and the reduction of a superoperator $\mathcal{O}$ as $\mathcal{O}^X = P_X\mathcal{O}P_X$, and $\mathcal{O}^{XY} = P_X\mathcal{O}P_Y$. Referring to Halati, Sheikhan, and Kollath [10], by only taking the contributions from the lowest lying subspace, one arrives at

$$\frac{\partial}{\partial t}\rho^0 = \mathcal{L}_0\rho^0 + \frac{1}{\hbar^2}P_0\left[H_\nu, (\mathcal{L}_0^{\Lambda_1})^{-1}P_1\left[H_\nu, \rho^0\right]\right], \tag{4.13}$$

where $\rho^0 \equiv \rho^{\Lambda_0}$ and P_0 and P_1 are the projectors to the decoherence free subspace and the excited subspace, respectively.

4.2.2 Perturbation in the fluctuations δH_{ac}

In this section, we want to apply the many-body adiabatic elimination method to our system after performing the mean-field decoupling in Sec. 4.1. We are going to treat the fluctuations δH_{ac}

as a perturbation around the dissipation free subspace referring to Bezvershenko et al. [11] and Halati [13]. The free Lindbladian is then given by

$$\mathcal{L}_0\rho = -\frac{i}{\hbar}\left[H_\mathrm{a}(\lambda) + H_\mathrm{c}(\Delta), \rho\right] + \frac{\Gamma}{2}\left(2a\rho a^\dagger - a^\dagger a\rho - \rho a^\dagger a\right). \tag{4.14}$$

For the dissipation free subspace, i.e. $\mathrm{Re}(\lambda_0) = 0$, a complete set of solutions to the eigenvalue equation $\mathcal{L}_0\rho^0 = \lambda_0\rho^0$ is given by elements of the form

$$\begin{aligned} \rho^0 &= \rho^0_\mathrm{a} \otimes \rho^0_\mathrm{c}, \\ \rho^0_\mathrm{a} &= |n_1(\lambda)\rangle \langle n_2(\lambda)|, \\ \rho^0_\mathrm{c} &= |\alpha(\Delta)\rangle \langle \alpha(\Delta)|, \end{aligned} \tag{4.15}$$

where the atomic part is determined by eigenstates $|n(\lambda)\rangle$ of H_a with energy $E_n(\lambda)$. As discussed previously, the cavity part ρ^0_c is given by a coherent state with the field

$$\alpha(\Delta) = \frac{\Omega}{\delta - i\Gamma/2}\Delta. \tag{4.16}$$

A general state in the decoherence free subspace can thus be written as

$$\rho^0 = |\alpha(\Delta)\rangle \langle \alpha(\Delta)| \otimes \rho^a(\lambda), \quad \text{with} \quad \rho^a = \sum_{n_1,n_2} c(n_1,n_2)\,|n_1(\lambda)\rangle \langle n_2(\lambda)|. \tag{4.17}$$

As mentioned at the beginning, we treat δH_ac as our perturbation. Hence, we have

$$\mathcal{V}(\rho) = -\frac{i}{\hbar}[\delta H_\mathrm{ac}, \rho] \tag{4.18}$$

and find for the time evolution the equation

$$\frac{\partial}{\partial t}\rho^0 = \mathcal{L}_0\rho^0 + \frac{1}{\hbar^2}P_0\left[\delta H_\mathrm{ac}, \mathcal{L}_0^{-1}P_1\left[\delta H_\mathrm{ac}, \rho^0\right]\right], \tag{4.19}$$

where we only consider the contributions from the lowest lying subspace as introduced in Eq. (4.13). Important to note is that compared to the mean-field approach, we will now avoid the arbitrary choice of just using the ground state of the effective model as our solution.

In order to derive the explicit form of the equation of motion, it is useful to first go to the shifted oscillator basis for the cavity operator, where we use the following notations

$$\begin{aligned} a = \tilde{a} + \alpha, \quad a^\dagger = \tilde{a}^\dagger + \alpha^*, \quad a + a^\dagger - \lambda = \tilde{a} + \tilde{a}^\dagger, \\ |0\rangle \equiv |\alpha\rangle, \quad \tilde{a}\,|0\rangle = 0, \quad |1\rangle \equiv \tilde{a}^\dagger\,|0\rangle, \text{ with } \langle 0|1\rangle = 0. \end{aligned} \tag{4.20}$$

In this basis, we can find some of the eigenstates of $\mathcal{L}_0$, which we will need later

$$\begin{aligned} &\mathcal{L}_0(|n,0\rangle \langle m,0|) = -i\Delta E_{n,m}/\hbar\,|n,0\rangle \langle m,0| \\ &\mathcal{L}_0(|n,1\rangle \langle m,0|) = [-i(\Delta E_{n,m}/\hbar + \delta) - \Gamma/2]\,|n,1\rangle \langle m,0|, \\ &\mathcal{L}_0(|n,0\rangle \langle m,1|) = [-i(\Delta E_{n,m}/\hbar - \delta) - \Gamma/2]\,|n,0\rangle \langle m,1|, \\ &\mathcal{L}_0(|n,0\rangle \langle m,2|) = [-i(\Delta E_{n,m}/\hbar - 2\delta) - \Gamma]\,|n,0\rangle \langle m,2|, \\ &\mathcal{L}_0(|n,0\rangle \langle m,0| - |n,1\rangle \langle m,1|) = (-i\Delta E_{n,m}/\hbar - \Gamma)(|n,0\rangle \langle m,0| - |n,1\rangle \langle m,1|), \end{aligned} \tag{4.21}$$

with $\Delta E_{n,m} = E_n - E_m$. We already see that the decoherence free subspace is spanned by states of the form $|n,0\rangle \langle m,0|$ and that the excited subspaces are spanned by states which have excitations in the state of the cavity field.

Now we can start by calculating the first commutator

$$\begin{aligned}\left[\delta H_{\mathrm{ac}}, \rho^0\right] &= -\hbar\Omega \left[\left(\tilde{a}+\tilde{a}^\dagger\right)\tilde{O}, \rho^0\right] \\ &= -\hbar\Omega \sum_{n_1,n_2} c(n_1,n_2)\left[\left(\tilde{a}+\tilde{a}^\dagger\right)\tilde{O}, |n_1,0\rangle\langle n_2,0|\right] \\ &= -\hbar\Omega \sum_{n_1,n_2} c(n_1,n_2)\left(\tilde{O}\,|n_1,1\rangle\langle n_2,0| - |n_1,0\rangle\langle n_2,1|\,\tilde{O}\right) \\ &= -\hbar\Omega \sum_{n_1,n_2} c(n_1,n_2)\sum_m \left(\tilde{O}_{n_1,m}\,|m,1\rangle\langle n_2,0| - \tilde{O}_{m,n_2}\,|n_1,0\rangle\langle m,1|\right),\end{aligned} \tag{4.22}$$

where $\tilde{O} = O - \Delta = O - \langle O\rangle_{\mathrm{a}}$. As the states $|n,1\rangle\langle m,0|$ and $|n,0\rangle\langle m,1|$ are already eigenstates of $\mathcal{L}_0$ in an excited subspace, the projector P_1 becomes the identity and the action of $\mathcal{L}_0^{-1}$ will give the inverse of the eigenvalues. In the next step, we need to compute the action of the second commutator leading to

$$\begin{aligned}\left[\left(\tilde{a}+\tilde{a}^\dagger\right)\tilde{O}, |m,1\rangle\langle n_2,0|\right] &= \sum_k \left(\tilde{O}_{m,k}\,|k,0\rangle\langle n_2,0| + \tilde{O}_{m,k}\,|k,2\rangle\langle n_2,0| - \tilde{O}_{k,n_2}\,|m,1\rangle\langle k,1|\right), \\ \left[\left(\tilde{a}+\tilde{a}^\dagger\right)\tilde{O}, |n_1,0\rangle\langle m,1|\right] &= \sum_k \left(\tilde{O}_{n_1,k}\,|k,1\rangle\langle m,1| - \tilde{O}_{k,m}\,|n_1,0\rangle\langle k,0| - \tilde{O}_{k,m}\,|n_1,0\rangle\langle k,2|\right).\end{aligned} \tag{4.23}$$

After that, we need to determine the action of the projector P_0 on the states which are not in the dissipation free subspace. For this, we write $|n,1\rangle\langle m,1| = |n,0\rangle\langle m,0| - (|n,0\rangle\langle m,0| - |n,1\rangle\langle m,1|)$, because we know that both of these two contributions are eigenstates of $\mathcal{L}_0$, where $|n,0\rangle\langle m,0|$ is a state in the dissipation free subspace and $|n,0\rangle\langle m,0| - |n,1\rangle\langle m,1|$ is in an excited subspace. Hence, we obtain that

$$P_0\,|n,1\rangle\langle m,1| = |n,0\rangle\langle m,0|\,. \tag{4.24}$$

The state $|n,0\rangle\langle m,0| - |n,1\rangle\langle m,1|$ is projected out by P_0 as this is an eigenstate of $\mathcal{L}_0$ with non-zero real part of the eigenvalue. The same argument holds for the state $|n,0\rangle\langle k,2|$. Thus we find that $P_0\,|n,0\rangle\langle k,2| = 0$.

Using these results, Eq. (4.19) becomes

$$\begin{aligned}\hbar\frac{\partial}{\partial t}\rho^0 = &-i\sum_{n_1,n_2}\Delta E_{n_1,n_2}c(n_1,n_2)\;\;|n_1,0\rangle\langle n_2,0| \\ &+\hbar^2\Omega^2\sum_{n_1,n_2}c(n_1,n_2)\sum_{m,k}\Big(\frac{1}{i\left(\Delta E_{n_2,m}-\hbar\delta\right)-\hbar\Gamma/2}\tilde{O}_{n_1,m}\tilde{O}_{m,k}\,|k,0\rangle\langle n_2,0| \\ &\qquad -\frac{1}{i\left(\Delta E_{n_2,m}-\hbar\delta\right)-\hbar\Gamma/2}\tilde{O}_{n_1,m}\tilde{O}_{k,n_2}\,|m,0\rangle\langle k,0| \\ &\qquad -\frac{1}{-i\left(\Delta E_{n_1,m}-\hbar\delta\right)-\hbar\Gamma/2}\tilde{O}_{m,n_2}\tilde{O}_{n_1,k}\,|k,0\rangle\langle m,0| \\ &\qquad +\frac{1}{-i\left(\Delta E_{n_1,m}-\hbar\delta\right)-\hbar\Gamma/2}\tilde{O}_{m,n_2}\tilde{O}_{k,m}\,|n_1,0\rangle\langle k,0|\Big).\end{aligned} \tag{4.25}$$

If we want to solve for the steady state, we obtain

$$\begin{aligned}0 = &-i\sum_{n_1,n_2}\Delta E_{n_1,n_2}c(n_1,n_2)\left|n_1,0\right\rangle\left\langle n_2,0\right| \\ &+\hbar^2\Omega^2\sum_{n_1,n_2}\sum_{m,k}\Big(c(k,n_2)\frac{1}{i\left(\Delta E_{n_2,m}-\hbar\delta\right)-\hbar\Gamma/2}\tilde{O}_{k,m}\tilde{O}_{m,n_1}\left|n_1,0\right\rangle\left\langle n_2,0\right| \\ &\qquad - c(m,k)\frac{1}{i\left(\Delta E_{k,n_1}-\hbar\delta\right)-\hbar\Gamma/2}\tilde{O}_{m,n_1}\tilde{O}_{n_2,k}\left|n_1,0\right\rangle\left\langle n_2,0\right| \\ &\qquad - c(k,m)\frac{1}{-i\left(\Delta E_{k,n_2}-\hbar\delta\right)-\hbar\Gamma/2}\tilde{O}_{n_2,m}\tilde{O}_{k,n_1}\left|n_1,0\right\rangle\left\langle n_2,0\right| \\ &\qquad + c(n_1,k)\frac{1}{-i\left(\Delta E_{n_1,m}-\hbar\delta\right)-\hbar\Gamma/2}\tilde{O}_{m,k}\tilde{O}_{n_2,m}\left|n_1,0\right\rangle\left\langle n_2,0\right|\Big),\end{aligned} \tag{4.26}$$

which gives

$$\begin{aligned}0 = -i\Delta E_{n_1,n_2}c(n_1,n_2) &+\hbar^2\Omega^2\sum_{m,k}\Big(c(k,n_2)\frac{1}{i\left(\Delta E_{n_2,m}-\hbar\delta\right)-\hbar\Gamma/2}\tilde{O}_{k,m}\tilde{O}_{m,n_1} \\ &- c(m,k)\frac{1}{i\left(\Delta E_{k,n_1}-\hbar\delta\right)-\hbar\Gamma/2}\tilde{O}_{m,n_1}\tilde{O}_{n_2,k} \\ &- c(k,m)\frac{1}{-i\left(\Delta E_{k,n_2}-\hbar\delta\right)-\hbar\Gamma/2}\tilde{O}_{n_2,m}\tilde{O}_{k,n_1} \\ &+ c(n_1,k)\frac{1}{-i\left(\Delta E_{n_1,m}-\hbar\delta\right)-\hbar\Gamma/2}\tilde{O}_{m,k}\tilde{O}_{n_2,m}\Big).\end{aligned} \tag{4.27}$$

Important to note here is that these equations no longer ensure that the solutions are positive semi-definite because they are obtained via a perturbative expansion.

Solving these equations for the full density matrix can be difficult simply because of the number of parameters $c(n_1,n_2)$ one has to solve for. Therefore, we present an ansatz for the atomic part of the density matrix, which reduces these degrees of freedom significantly in the following. We first calculate the evolution of the atomic energy H_a,

$$\begin{aligned}\frac{\partial}{\partial t}\left\langle H_\mathrm{a}\right\rangle &= \mathrm{Tr}\left(H_\mathrm{a}\frac{\partial}{\partial t}\rho^0\right) \\ &= \hbar\Omega^2\sum_{n_1,n_2}c(n_1,n_2)\sum_m\Big(\frac{1}{i\left(\Delta E_{n_2,m}-\hbar\delta\right)-\hbar\Gamma/2}\tilde{O}_{n_1,m}\tilde{O}_{m,n_2}E_{n_2} \\ &\qquad - \frac{1}{i\left(\Delta E_{n_2,m}-\hbar\delta\right)-\hbar\Gamma/2}\tilde{O}_{n_1,m}\tilde{O}_{m,n_2}E_m \\ &\qquad - \frac{1}{-i\left(\Delta E_{n_1,m}-\hbar\delta\right)-\hbar\Gamma/2}\tilde{O}_{m,n_2}\tilde{O}_{n_1,m}E_m \\ &\qquad + \frac{1}{-i\left(\Delta E_{n_1,m}-\hbar\delta\right)-\hbar\Gamma/2}\tilde{O}_{m,n_2}\tilde{O}_{n_1,m}E_{n_1}\Big),\end{aligned} \tag{4.28}$$

which simplifies to

$$\begin{aligned}\frac{\partial}{\partial t}\left\langle H_\mathrm{a}\right\rangle = \hbar\Omega^2\sum_{n_1,n_2}c(n_1,n_2)\sum_m\Bigg(&\frac{1}{i\left(\Delta E_{n_2,m}-\hbar\delta\right)-\hbar\Gamma/2}\Delta E_{n_2,m} \\ &- \frac{1}{i\left(\Delta E_{n_1,m}-\hbar\delta\right)+\hbar\Gamma/2}\Delta E_{n_1,m}\Bigg)\tilde{O}_{m,n_2}\tilde{O}_{n_1,m}.\end{aligned} \tag{4.29}$$

If we now assume that the density matrix is well described by a thermal state $\rho^a \sim \exp(-\beta H_\mathrm{a}(\lambda))$, then the energy transfer can be simplified a lot more. This assumption is valid if the atomic system is interacting such that it can thermalize and if the thermalization time of the atomic

system is short compared to the time-scale induced by scattering from photon fluctuations. For $c(n_1, n_2) = c_{n_1}\delta_{n_1,n_2}$ with $c_n = e^{-\beta E_n}/Z$, the energy transfer becomes

$$\begin{aligned}\frac{\partial}{\partial t}\langle H_\mathrm{a}\rangle &= \frac{\hbar\Omega^2}{Z}\sum_{n,m} e^{-\beta E_n}|\tilde{O}_{m,n}|^2\Delta E_{n,m}\left(\frac{1}{i\left(\Delta E_{n,m}-\hbar\delta\right)-\hbar\Gamma/2}-\frac{1}{i\left(\Delta E_{n,m}-\hbar\delta\right)+\hbar\Gamma/2}\right)\\ &= -\frac{\hbar^2\Omega^2}{Z}\sum_{n,m}|\langle n|O-\langle O\rangle_\mathrm{a}|m\rangle|^2 e^{-\beta E_n}\Delta E_{n,m}\frac{\Gamma}{\left(\Delta E_{n,m}-\hbar\delta\right)^2+\left(\hbar\Gamma/2\right)^2} \qquad (4.30)\\ &= \frac{\hbar^2\Omega^2}{Z}\sum_{n,m}|\langle n|O-\langle O\rangle_\mathrm{a}|m\rangle|^2 e^{-\beta E_m}\Delta E_{n,m}\frac{\Gamma}{\left(\Delta E_{n,m}+\hbar\delta\right)^2+\left(\hbar\Gamma/2\right)^2}.\end{aligned}$$

In the steady state, the left hand side vanishes and we only have to solve for the temperature $T = 1/k_B\beta$ by additionally fulfilling the self-consistency condition Eq. (4.7). The eigenstates $|n\rangle$ of H_a with the corresponding energies E_n are obtained via exact diagonalization of H_a. Further, note that the thermal state ansatz automatically fulfills the positive semi-definiteness of our solution. In Chapter 6 and Chapter 7, we will use the equations derived in this section in order to find the steady state solution of our system.

5 Integrability of the atomic mean-field Hamiltonian

Before we go on with our study of the self-organization transition, we first want to investigate the atomic mean-field Hamiltonian further, which is also called ionic Hubbard model in the literature. In Chapter 4, we introduced a thermal ansatz for the atomic part of the density matrix. Important for the applicability of this ansatz is that the underlying system thermalizes. According to Kollath et al. [15] and references therein, it is believed that this requires the system to be non-integrable which motivates the following analysis[1].

5.1 Theory of level-statistics and symmetries

The ionic Hubbard Hamiltonian consists of that of the one-dimensional Hubbard model, which is an integrable model as shown by Lieb and Wu in 1968 [17], and an additional alternating potential term, i.e.

$$H = -J\sum_{j=1}^{L}\sum_{\sigma\in\{\uparrow,\downarrow\}}(c_{j,\sigma}^{\dagger}c_{j+1,\sigma} + c_{j+1,\sigma}^{\dagger}c_{j,\sigma}) + U\sum_{j=1}^{L} n_{j,\uparrow}n_{j,\downarrow} - \hbar\eta\sum_{j=1}^{L}\sum_{\sigma\in\{\uparrow,\downarrow\}}(-1)^{j}n_{j,\sigma}, \tag{5.1}$$

where we now define η as the strength of the potential. Note that we use periodic boundary conditions, i.e. $L+1\widehat{=}1$. Now we want to investigate whether this additional alternating potential term breaks the integrability of the Hubbard model. For this, we follow Poilblanc et al. [18] and Kollath et al. [15] and use an approach which is based on the spectral properties of the Hamiltonian. One considers the set of energies E_n in ascending order and defines the gap between adjacent energies as

$$\delta_n = E_{n+1} - E_n. \tag{5.2}$$

If the underlying model is integrable, then these level-spacings exhibit a Poissonian distribution, i.e. $P(\delta/\Delta) = \exp(-\delta/\Delta)$. In contrast, the distribution of the level-spacings takes the form $P(\delta/\Delta) = \frac{\pi}{2}\frac{\delta}{\Delta}\exp\left(-\frac{\pi}{4}\frac{\delta^2}{\Delta^2}\right)$ if the model is non-integrable meaning that the model has similar universal features as the Gaussian orthogonal ensemble (GOE). In both cases, Δ is the mean level-spacing. In our disscusion of the integrability, we use another quantity defined by

$$r_n = \min(\delta_n, \delta_{n-1})/\max(\delta_n, \delta_{n-1}). \tag{5.3}$$

Since these ratios of consecutive level-spacings are independent of the local density of states, this quantity does not require an unfolding procedure. The probability that these ratios of consecutive level-spacings lie between r and $r+\mathrm{d}r$ is given by $P(r)\mathrm{d}r$. For a Poissonian distribution, one finds $P(r) = 1/(1+r)^2$. For the GOE, one finds $P(r) = \frac{27}{4}\frac{r+r^2}{(1+r+r^2)^{1+(3/2)}}$ (see Atas et al. [19]).

For our analysis, we need to take the symmetries of our model into account and restrict the computation of the distribution $P(r)$ to the different symmetry sectors. Note that remaining symmetries influence the resulting distribution which will be discussed in more detail in the case of half-filling (see Giraud et al. [20]). The Hamiltonian has the following symmetries:

Particle number conservation The particle number operator is given by $N = \sum_{i=1}^{L}\sum_{\sigma} c_{i,\sigma}^{\dagger}c_{i,\sigma}$. The corresponding symmetry sectors are given by a fixed particle number N and are labled accordingly.

[1] Note that Hosseinzadeh and Jafari [16] have recently claimed that the ionic Hubbard model is integrable.

SU(2) symmetry The SU(2) symmetry is generated by the operators

$$S_\alpha = \frac{\hbar}{2} \sum_{i=1}^{L} (c_{i,\uparrow}^\dagger, c_{i,\downarrow}^\dagger)\, \sigma_\alpha \begin{pmatrix} c_{i,\uparrow} \\ c_{i,\downarrow} \end{pmatrix} \tag{5.4}$$

for $\alpha = x, y, z$, where σ_α are the Pauli matrices. For the different symmetry sectors, we fix the quantum number j of the total spin S^2 and the quantum number m of the S_z operator. Note that, by abuse of notation we write $S = j$ and $S_z = m$.

Translation symmetry The translation symmetry T is defined as the unique unitary operator that leaves the vacuum invariant and acts on the annihilation operators by $Tc_{i,\sigma}T^\dagger = c_{i+2,\sigma}$. The eigenvalues of this operator are given by $\exp(2\pi ik/(L/2))$ with $k = 0, \ldots, L/2-1$ and we use k to label the symmetry sector.

Reflection symmetry The reflection[2] symmetry R is defined as the unique unitary operator that leaves the vacuum invariant and acts on the annihilation operators by $Rc_{i,\sigma}R^\dagger = c_{2-i,\sigma}$. The associated symmetry sectors are labeled by $R = \pm$.

It is straight forward to see that all of these operators commute with the Hamiltonian. We further see that all pairs except for (T, R) commute with each other. However, the action of R can be restricted to the eigenspaces with $T = \pm 1$ and hence in these eigenspaces we can consider the action of both T and R simultaneously.

For the calculation of the eigenvalues of our Hamiltonian in the different symmetry sectors, a code provided by Prof. Dr. Andreas Läuchli was used. Note that this code does the decomposition only into symmetry blocks with respect to the symmetries N, S_z, T and R (for $T = \pm 1$). This is sufficient since the S^2 quantum numbers can be reconstructed as follows. The highest S_z quantum number tells us how many multiplets with maximal S^2 occur. For each of these multiplets, we then remove the associated energy eigenvalue once from each symmetry block with lower S_z quantum number. We repeat the procedure until we have reconstructed all S^2 quantum numbers together with their multiplicities.

Since the behavior of the level-statistics is independent of the chosen symmetry sector, we use the one containing the largest number of eigenenergies for our analysis[3] [18].

[2] We make the arbitrary choice of reflecting around the first site. All other reflections can be generated by invoking translations.

[3] Note that we confirmed this by looking at the level-statistics in every symmetry sector for several examples.

5.2 Level-statistics for quarter-filling

Starting with the case of quarter-filling, i.e. $N/L = 1/2$, we first want to benchmark our results. For this, we go into the limit of $\eta \to 0$, where we expect to see a Poissonian distribution since the one-dimensional Hubbard model is integrable [17]. Fig. 5.1 shows the resulting distribution in comparison to the Poissonian distribution and the GOE distribution[4].

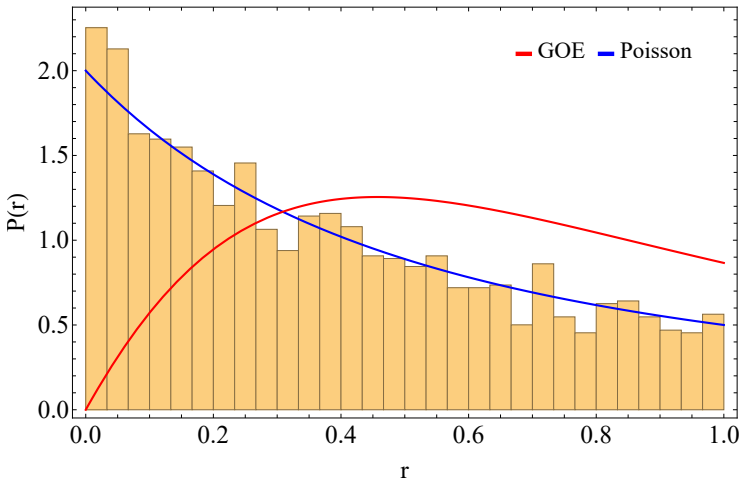

Figure 5.1: Distribution of the ratios of consecutive level-spacings for $N = 6$, $L = 12$ for the symmetry sector $S = 1$, $S_z = 0$, $k = 1$ by using 30 bins. The parameters of the system are $U/J = 2$ and $\hbar\eta/J = 0$. The mean value is given by $\langle r \rangle = 0.3756$.

One clearly sees that the ratios of consecutive level-spacings follow a Poissonian distribution as expected. One can verify this even more by looking at the mean value of r. For the Poissonian distribution, it is given by $\langle r \rangle_{\mathrm{P}} = 0.386$ [15] and for the GOE, it is $\langle r \rangle_{\mathrm{GOE}} = 0.531$ [15]. Our statistics yield $\langle r \rangle = 0.3756$ which is also in good agreement with the mean value of the Poissonian distribution.

Now we want to see whether the situation changes if we start to increase the strength of the staggered potential. This can be seen in Fig. 5.2 for $\hbar\eta/J = 1$.

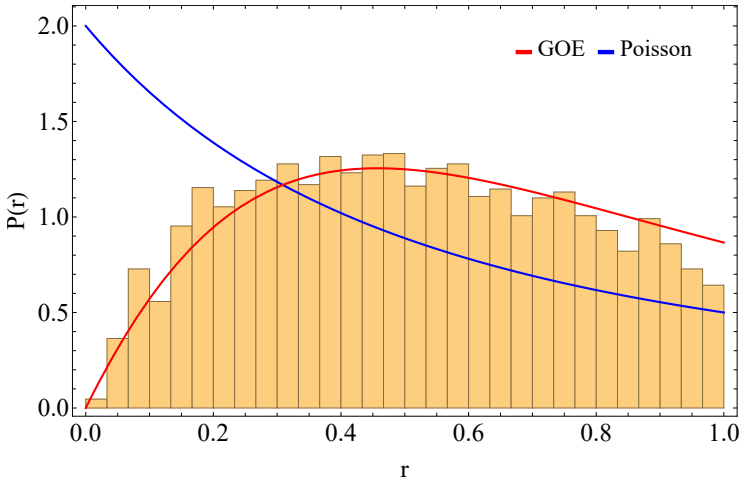

Figure 5.2: Distribution of the ratios of consecutive level-spacings for $N = 6$, $L = 12$ for the symmetry sector $S = 1$, $S_z = 0$, $k = 1$ by using 30 bins. The parameters of the system are $U/J = 2$ and $\hbar\eta/J = 1$. The mean value is given by $\langle r \rangle = 0.5149$.

[4]Note that for the following discussion the binning was choosen such that every bin contains at least one value.

We can observe a very distinct behavior, i.e. the ratios of consecutive level-spacings follow a GOE distribution. Again, we can also have a look at the mean value given by $\langle r \rangle = 0.5149$ which is now in good agreement with the one of the GOE, which is $\langle r \rangle_{\mathrm{GOE}} = 0.531$. This already shows that the staggered potential breaks the integrability of the one-dimensional Fermi-Hubbard model and causes a GOE like level statistics.

In order to support this, we performed this analysis for a variety of different parameter sets. Fig. 5.3 shows the calculated mean values of r for different parameter sets in comparison to the mean values of the Poissonian distribution and the GOE distribution.

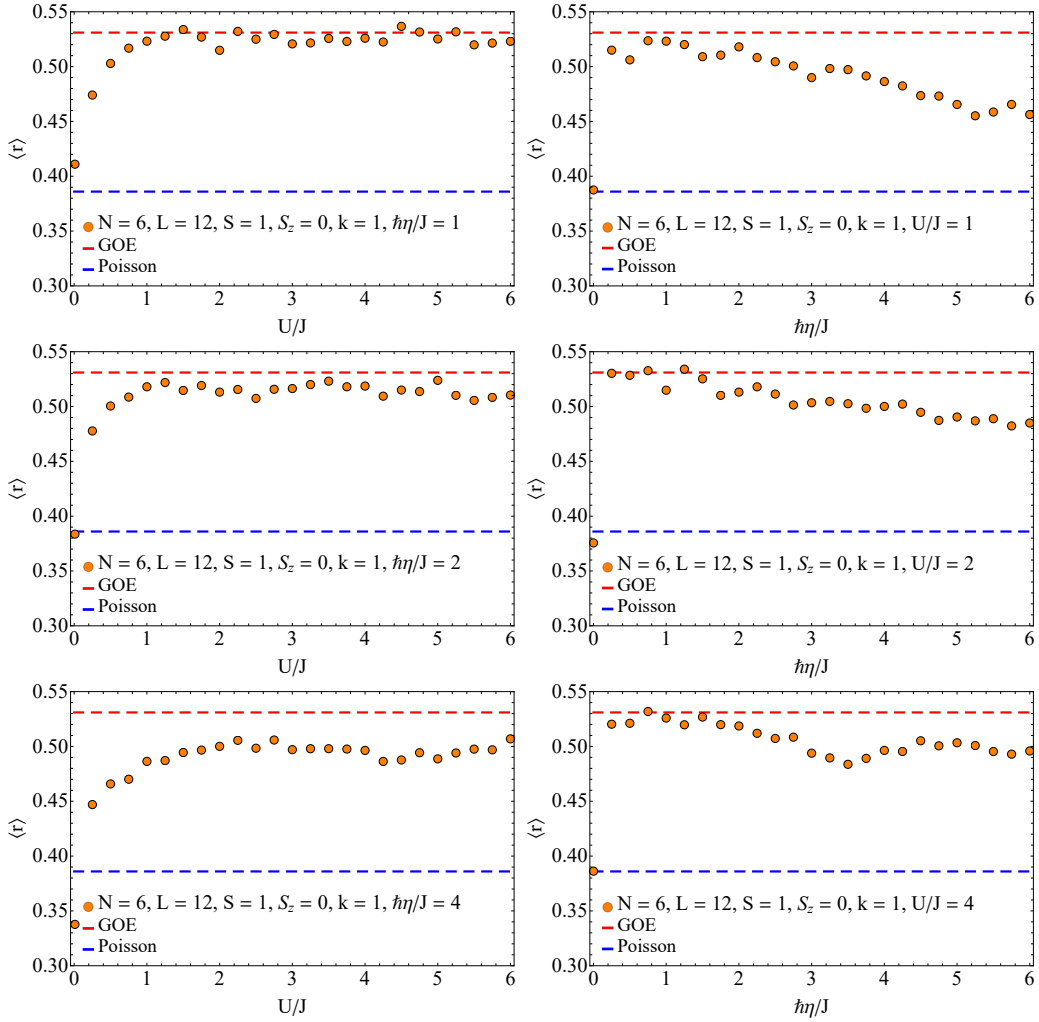

Figure 5.3: Evolution of the mean value $\langle r \rangle$ of the ratios of consecutive level-spacings with the interaction strength U or with the strength of the staggered potential η. For the Poissonian distribution, the mean value is given by $\langle r \rangle_{\mathrm{P}} = 0.386$ and for the GOE distribution, the mean value is $\langle r \rangle_{\mathrm{GOE}} = 0.531$ [15].

For most of the parameters, in particular in the case of fixing the strength of the potential to $\hbar\eta/J = 1$ and varying the interaction strength U, we see a good agreement with the value predicted for a GOE distribution. While the behavior is very stable against variations of U deviations can especially be seen for small and large values of η. In these cases, we assume that the deviations are due to finite size effects. In order to verify this, we consider a bigger system, i.e. $N = 8$ and $L = 16$, and calculate the mean values $\langle r \rangle$ of the ratios of consecutive level-spacings in a parameter regime in which the deviations were most prominent. The result can be seen in Fig. 5.4.

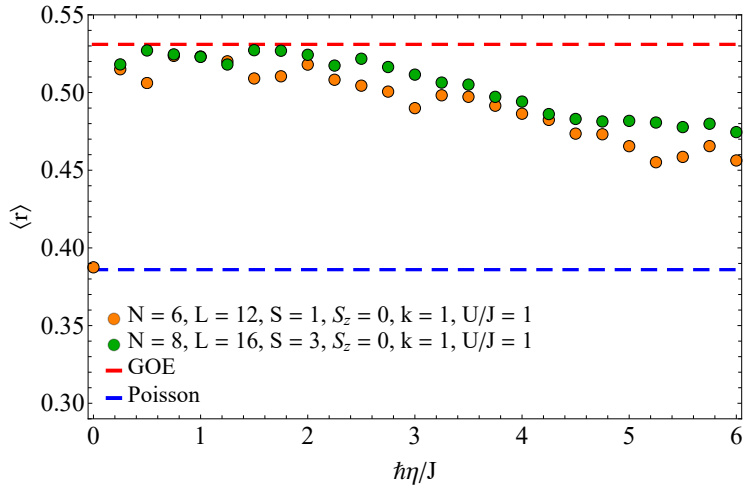

Figure 5.4: Evolution of the mean value $\langle r \rangle$ of the ratios of consecutive level-spacings with the strength of the staggered potential η. For the Poissonian distribution, the mean value is given by $\langle r \rangle_{\mathrm{P}} = 0.386$ and for the GOE distribution, the mean value is $\langle r \rangle_{\mathrm{GOE}} = 0.531$ [15].

One observes that the mean values $\langle r \rangle$ for the bigger system are closer to the mean value of the GOE distribution than the ones for the smaller system. Hence, one can expect that the mean values of bigger system sizes will tend even more to the mean value of the GEO distribution and that the origin of the deviations are finite size effects.

In summary, this analysis confirms our previous observation and leads to the conclusion that the model is non-integrable.

5.3 Level-statistics for half-filling

In contrast to the case of quarter-filling, the situation changes for half-filling, i.e. $N/L = 1$. One example for the distribution $P(r)$ is depicted in Fig. 5.5. The distribution neither follows a GOE distribution nor a Poissonian distribution.

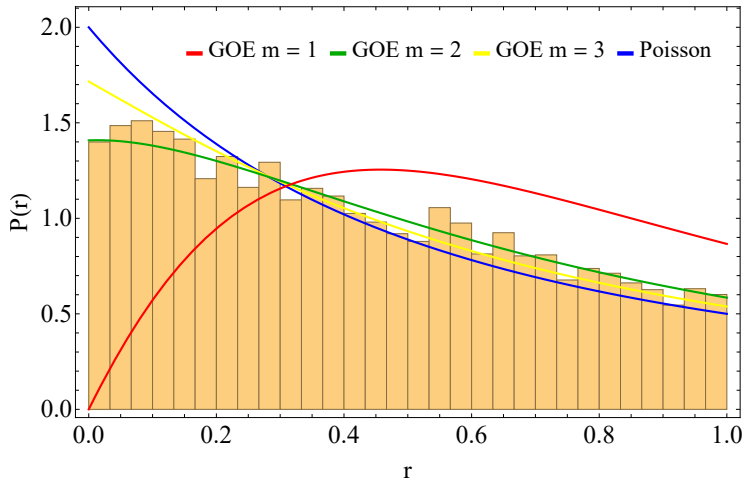

Figure 5.5: Distribution of the ratios of consecutive level-spacings for $N = 10$, $L = 10$ for the symmetry sector $S = 1$, $S_z = 0$, $k = 1$ by using 30 bins. The parameters of the system are $U/J = 2$ and $\hbar\eta/J = 1$. The mean value is given by $\langle r \rangle = 0.4190$.

Note that the same parameters were used as in the example shown in Fig. 5.2 for quarter-filling, where the distribution clearly follows a GOE distribution. We attribute this behavior to the presence of another symmetry in the case of half-filling, which is a particle hole symmetry associated with the transformation $c_{i,\sigma} \rightarrow (-1)^i c^\dagger_{i+1,\sigma}$. This symmetry is not implemented in the exact diagonalization code yet. Referring to Giraud et al. [20], the distribution related to the GOE changes according to the number of symmetries that were not taken into account. In particular, the number of symmetry blocks can be determined by the mean value $\langle r \rangle$ of the distribution. As we already know that the particle hole symmetry is missing so far, which would lead to a further splitting into two blocks of equal size, we can see whether this is the only symmetry which is missing in our analysis. Moreover, this would then mean that we can expect to find a clear GOE behavior if one would implement this additional symmetry showing again the non-integrability of the ionic Hubbard model. Because of the fact that the parameter regime for $\hbar\eta/J = 1$ and $U/J \in (0, 6]$ was suffering at least under finite size effects in our previous analysis, we use this regime in the following. Fig. 5.6 shows the resulting evolution of the mean value of the ratios of consecutive level spacings $\langle r \rangle$ with the interaction strength. If a further splitting into two blocks of equal size, labled by m, is possible, the mean value should be $\langle r \rangle_{\mathrm{GOE},m=2} = 0.4234$ [20]. If one could divide further into three blocks of equal size, the mean value should be $\langle r \rangle_{\mathrm{GOE},m=3} = 0.4033$ [20]. For more missing symmetries, the mean value approaches the one of the Poissonian distribution. Our data is in good agreement with $\langle r \rangle_{\mathrm{GOE},m=2} = 0.4234$ which suggests that the particle hole symmetry mentioned at the beginning is the only one missing in our analysis. Going back to Fig. 5.5, we can also compare the resulting distribution $P(r)$ to the one of the GOE with $m = 2$ and $m = 3$. Especially at $P(0)$, we see that the distribution agrees well with the GOE distribution for $m = 2$, where $P_2(0) = 1.4081$ [20], and hence disagrees with $P_3(0) = 1.7159$ for the GOE distribution for $m = 3$ [20]. All in all, this suggests also the conclusion that the ionic Hubbard model is non-integrable.

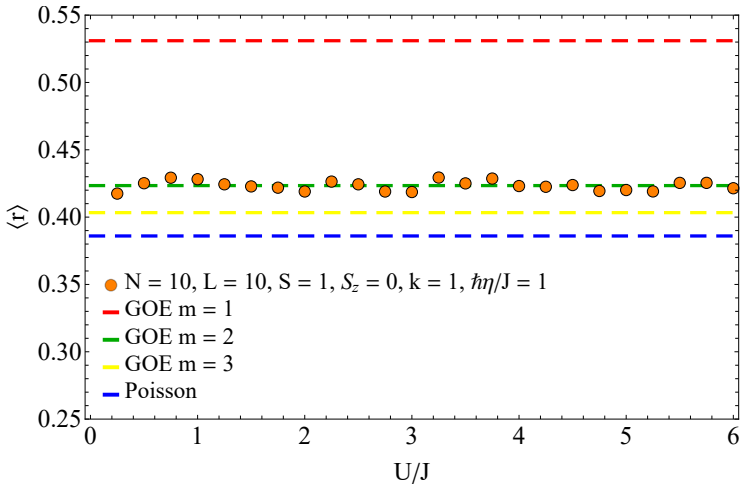

Figure 5.6: Evolution of the mean value $\langle r \rangle$ of the ratios of consecutive level-spacings with the interaction strength U. For the Poissonian distribution, the mean value is given by $\langle r \rangle_{\mathrm{P}} = 0.386$ and for the GOE distribution the mean value is $\langle r \rangle_{\mathrm{GOE},m=1} = 0.531$ [15]. For $m = 2$ symmetry blocks, the mean value is $\langle r \rangle_{\mathrm{GOE},m=2} = 0.4234$ and for $m = 3$, the mean value is given by $\langle r \rangle_{\mathrm{GOE},m=3} = 0.4033$ [20].

Another possibility of showing that the particle hole symmetry prevents us from obtaining a clear GOE distribution is given by a small change in the Hamiltonian. By changing the interaction term to

$$H_{\mathrm{int}} = U_0 \sum_{j=1}^{L/2} n_{2j,\uparrow} n_{2j,\downarrow} + U_1 \sum_{j=1}^{L/2} n_{2j+1,\uparrow} n_{2j+1,\downarrow} \tag{5.5}$$

one breaks the particle hole symmetry but the other symmetries remain valid. Fig. 5.7 shows an example of the resulting distribution using a finite difference of the interaction strengths $U_1 - U_0 =$

1. The resulting mean value of the distribution is given by $\langle r \rangle = 0.5297$. This is now again in good agreement with the distribution of the GOE.

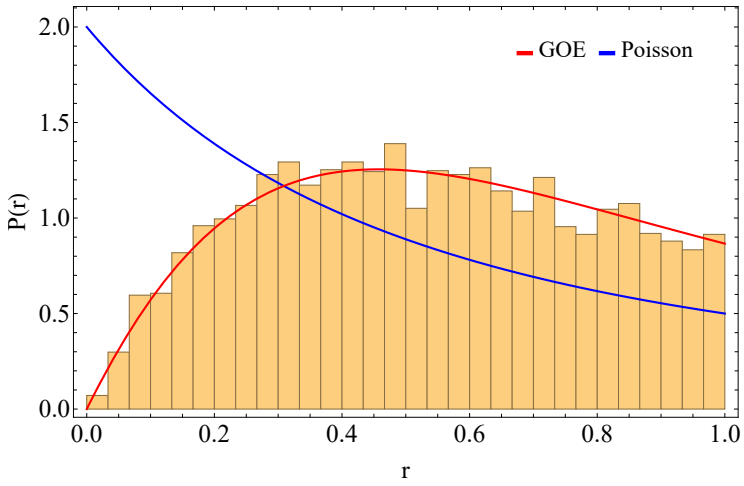

Figure 5.7: Distribution of the ratios of consecutive level-spacings for $N = 10$, $L = 10$ for the symmetry sector $S = 1$, $S_z = 0$, $k = 1$ by using 30 bins. The parameters of the system are $U_0/J = 1$, $U_1/J = 2$ and $\hbar\eta/J = 1$. The mean value is given by $\langle r \rangle = 0.5297$.

Again, we have a look at a few more examples by comparing the resulting mean values $\langle r \rangle$ of the ratios of consecutive level-spacings with the mean values of the different possible distributions. In the limit of $U_1 - U_0 \to 0$, we expect to see an agreement with the mean-value of the GOE distribution for $m = 2$ since the particle hole symmetry is not broken anymore. Fig. 5.8 shows the resulting evolution of the mean value $\langle r \rangle$ with the difference of the interaction strengths $U_1 - U_0$. For most of the differences of the interaction strengths, we see a good agreement with the mean value of the GOE distribution. Only in the limit of $U_1 - U_0 \to 0$, we observe that the mean value approaches the one of the GOE distribution for $m = 2$, as expected.

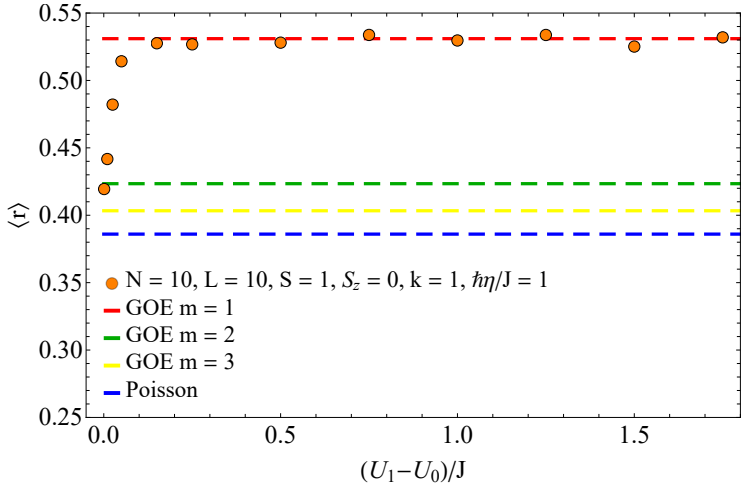

Figure 5.8: Evolution of the mean value $\langle r \rangle$ of the ratios of consecutive level-spacings with the difference of the interaction strengths $U_1 - U_0$. For the Poissonian distribution, the mean value is given by $\langle r \rangle_{\mathrm{P}} = 0.386$ and for the GOE distribution, the mean value is $\langle r \rangle_{\mathrm{GOE},m=1} = 0.531$ [15]. For $m = 2$ symmetry blocks, the mean value is $\langle r \rangle_{\mathrm{GOE},m=2} = 0.4234$ and for $m = 3$, the mean value is given by $\langle r \rangle_{\mathrm{GOE},m=3} = 0.4033$ [20].

To conclude, we expect a distribution, which follows the one of the GOE after implementing the particle hole symmetry. This suggests again the non-integrability of the ionic Hubbard model.

6 The non-interacting system

We start our study of the self-organization transition for the system introduced in Chapter 3 in Eq. 3.9 in the non-interacting case, i.e. $U = 0$. Thus, in the following we can also neglect the spin degree of freedom. Here, we will first introduce the concept of symmetries in the case of open quantum systems. This will then allow us to study the influence of a strong symmetry on the nature of the steady state of this system.

6.1 Solving the eigenvalue equation for the atomic part

In the case of non-interacting fermions, we are able to analytically solve the eigenvalue equation $H_a(\lambda)\,|n(\lambda)\rangle = E_n(\lambda)\,|n(\lambda)\rangle$ for the atomic mean-field Hamiltonian. We start by using a Fourier transformation to write the Hamiltonian in momentum space. Assuming periodic boundary conditions, the transformation reads

$$c_j^\dagger = \frac{1}{\sqrt{L}} \sum_{m=1}^{L} e^{2\pi i m j/L} c_m^\dagger. \tag{6.1}$$

One finds

$$H_a(\lambda) = -2J \sum_k \cos(k) c_k^\dagger c_k - \hbar\Omega\lambda \sum_k c_k^\dagger c_{k+\pi}, \tag{6.2}$$

where the momentum of the atoms is given by $k_m = \frac{2\pi m}{L}$ with $m = 1, \ldots, L$. In this basis, one sees that the coupling between the atoms and the cavity field introduces a coupling only between the atoms with momentum k and $k + \pi$. We can now diagonalize this Hamiltonian by using the canonical transformation

$$\begin{aligned} c_k^\dagger &= u_k a_k^\dagger + v_k b_k^\dagger, \\ c_{k+\pi}^\dagger &= v_k a_k^\dagger - u_k b_k^\dagger, \\ u_k^2 + v_k^2 &= 1, \end{aligned} \tag{6.3}$$

where we restrict to the momenta $k_m = \frac{2\pi m}{L}$ with $m = 1, \ldots, L/2$ and $u_k,\ v_k \in \mathbb{R}$. Then the operators a and b fulfill the usual fermionic anti-commutation relations. Choosing

$$\begin{aligned} u_k &= \frac{1}{\sqrt{2}} \sqrt{1 - \frac{2J\cos(k)}{\sqrt{(\hbar\Omega\lambda)^2 + (2J\cos(k))^2}}} \\ v_k &= -\frac{1}{\sqrt{2}} \sqrt{1 + \frac{2J\cos(k)}{\sqrt{(\hbar\Omega\lambda)^2 + (2J\cos(k))^2}}}. \end{aligned} \tag{6.4}$$

the Hamiltonian has the diagonal form

$$H_a(\lambda) = \sum_k E_k (a_k^\dagger a_k - b_k^\dagger b_k) \quad \text{with} \quad E_k = \sqrt{(2J\cos(k))^2 + (\hbar\Omega\lambda)^2}. \tag{6.5}$$

In this basis, the imbalance operator O reads

$$O = \sum_k (2u_k v_k a_k^\dagger a_k - 2u_k v_k b_k^\dagger b_k + (v_k^2 - u_k^2)(a_k^\dagger b_k + b_k^\dagger a_k)) \tag{6.6}$$

and hence $\tilde{O}$ is given by

$$\tilde{O} = \sum_k (2u_k v_k a_k^\dagger a_k - 2u_k v_k b_k^\dagger b_k + (v_k^2 - u_k^2)(a_k^\dagger b_k + b_k^\dagger a_k)) - \frac{\delta^2 + \Gamma^2/4}{2\Omega\delta} \lambda\, \mathbb{1}. \tag{6.7}$$

6.2 Symmetries of the Lindblad master equation

In closed quantum systems with a unitary time evolution, a symmetry of the Hamiltonian implies a conserved quantity. For a hermitian, not explicitly time-dependent observable S, the following statements are equivalent

$$[S, H] = 0 \Leftrightarrow U^\dagger H U \Leftrightarrow \frac{\mathrm{d}}{\mathrm{d}t}\langle S\rangle = 0, \tag{6.8}$$

where a continuous symmetry is given by $U = e^{i\phi S}$ for $\phi \in \mathbb{R}$. Following Albert and Jiang [21], and Buča and Prosen [22], in an open quantum system described by the Lindblad master equation, a symmetry of the Liouvillian does not always imply a conserved quantity. One distinguishes in this case between a weak and a strong symmetry. A weak symmetry is classified by the condition $\mathcal{L}(U\rho U^\dagger) = U\mathcal{L}(\rho)U^\dagger$ with O being a hermitian operator generating the symmetry $U = e^{i\phi O}$ for $\phi \in \mathbb{R}$. In contrast to the situation before, this does not imply the existence of a conserved quantity. A strong symmetry, which implies the existence of a conserved quantity, additionally requires that the operator O is commuting with the Hamiltonian and all jump operators J_m. Hence, the following holds

$$\mathcal{L}(U\rho U^\dagger) = U\mathcal{L}(\rho)U^\dagger \Leftarrow [O, H] = 0 = [O, J_m] \ \ \forall m \Rightarrow \frac{\mathrm{d}}{\mathrm{d}t}\langle O\rangle = 0. \tag{6.9}$$

In contrast to a weak symmetry, a strong symmetry further gives rise to multiple steady states in the system.

In the non-interacting case, we have written down the atomic mean-field Hamiltonian in momentum space in Eq. (6.2) showing us that we only have a coupling between the momentum states k and $k + \pi$. Based on this, we find that the operator

$$O_{k_j} = c^\dagger_{k_j} c_{k_j} + c^\dagger_{k_j+\pi} c_{k_j+\pi} \quad \text{for} \quad j = 1, \ldots, L/2 \tag{6.10}$$

leads to a strong symmetry in our system because $[H_c, O_{k_j}] = [H_a, O_{k_j}] = [a, O_{k_j}] = 0$ holds. This means that the expectation values $\langle O_{k_j}\rangle = m_{k_j}$ are conserved quantities. This is in contrast to the interacting case, were the atomic Hamiltonian does not commute anymore with this operator since $[H_{\mathrm{int}}, O_{k_j}] \neq 0$. In the presence of this symmetry, we can now block diagonalize the Liouvillian in different symmetry sectors, were each of these sectors will contain at least one steady state. In the single particle case, these symmetry sectors will be spanned by the momentum states $|k_j\rangle$ and $|k_j + \pi\rangle$ for $j = 1, \ldots, L/2$ leading to $L/2$ independent symmetry sectors. For N atoms, we can generalize this and label each symmetry sector by $(m_{k_1}, m_{k_2}, \ldots, m_{k_{L/2}})$ with $\sum_{i=1}^{L/2} m_{k_i} = N$. This means that the symmetry sectors in the multi-particle case are given by the different combinations in which the atoms can be arranged in the single particle sectors. Based on this observations, we will study the different steady states which arise in our non-interacting system in the following. Note that the introduced strong symmetry was already investigated for bosonic atoms coupled to a cavity by Halati, Sheikhan, and Kollath [12].

6.3 Steady state solutions

In order to find the solutions for the density matrix in the steady state, we use Eq. (4.27) as our starting point, meaning that we include the fluctuations of the mean-field approach within the many-body adiabatic elimination. Further, we solve for every entry of the density matrix since no interactions are present in our current model making the thermal ansatz $\rho^a \sim \exp(-\beta H_{\mathrm{a}}(\lambda))$ inapplicable. For this, we rewrite Eq. (4.27) into a matrix equation of the form

$$M \cdot \rho = 0, \tag{6.11}$$

where ρ now represents a vector containing the components of the density matrix. The components of the resulting matrix M are given by

$$\begin{aligned} M_{n_1 n_2, ij} = &-i\Delta E_{n_1,n_2}\delta_{i,n_1}\delta_{j,n_2} + \hbar^2\Omega^2\delta_{j,n_2}\sum_m \frac{1}{i\left(\Delta E_{n_2,m} - \hbar\delta\right) - \hbar\Gamma/2}\tilde{O}_{i,m}\tilde{O}_{m,n_1} \\ &+ \hbar^2\Omega^2\delta_{i,n_1}\sum_m \frac{1}{-i\left(\Delta E_{n_1,m} - \hbar\delta\right) - \hbar\Gamma/2}\tilde{O}_{m,j}\tilde{O}_{n_2,m} \\ &- \hbar^2\Omega^2\frac{1}{i\left(\Delta E_{j,n_1} - \hbar\delta\right) - \hbar\Gamma/2}\tilde{O}_{i,n_1}\tilde{O}_{n_2,j} \\ &- \hbar^2\Omega^2\frac{1}{-i\left(\Delta E_{i,n_2} - \hbar\delta\right) - \hbar\Gamma/2}\tilde{O}_{n_2,j}\tilde{O}_{i,n_1}. \end{aligned} \tag{6.12}$$

We further use the basis in which the atomic Hamiltonian is diagonal as derived in Sec. 6.1. The steady states of the system can now be found by first restricting this matrix M to the symmetry sectors introduced in the previous section. After that, one calculates the kernel of M in each sector which yields our solution. Since we also need to fulfill the self-consistency condition (see Eq. 4.7), we vary the input λ_{in}, i.e. the passed mean-field value of the cavity field, for a fixed set of parameters ($\hbar\delta/J$, $\hbar\Gamma/J$, $\hbar\Omega/J$) until the output λ_{out}, i.e. the mean-field of the cavity calculated with the obtained steady state solution, matches the input λ_{in}. Fig. 6.1 depicts the procedure for different Ω. One can see that for low coupling strengths, e.g. for $\hbar\Omega/J = 1$, the self-consistency equation is only fulfilled at $\lambda = 0$. For higher coupling strengths, the self-consistency equation is also fulfilled for a finite λ, which marks the transition to the self-organized phase. In this case, the solution for $\lambda = 0$ is unstable and will hence be discarded [23].

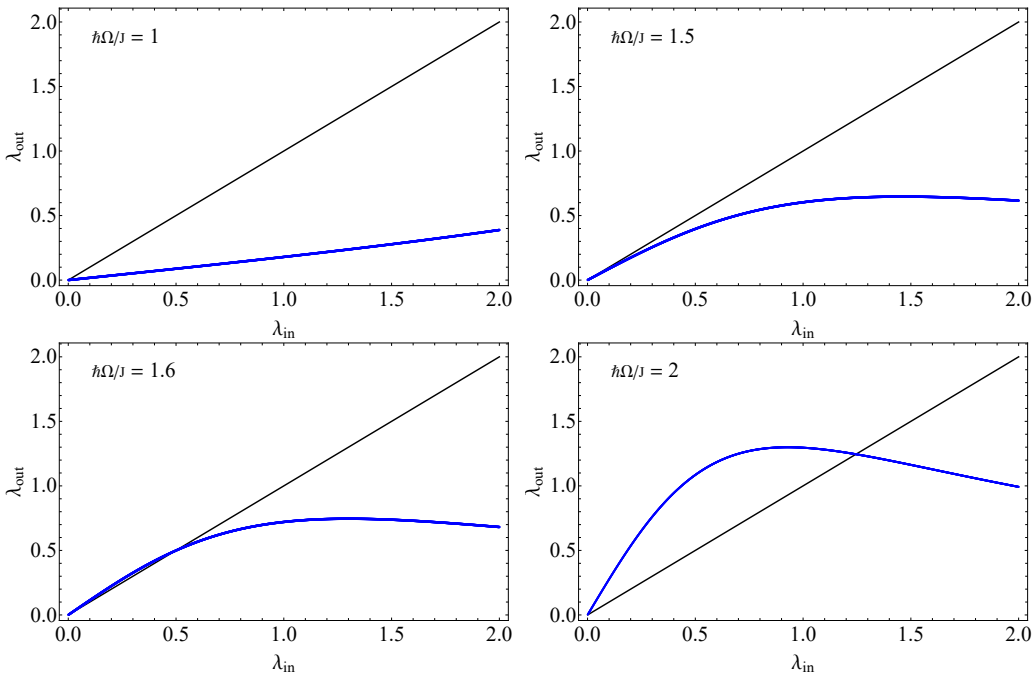

Figure 6.1: Illustration of computing the value of λ in order to fulfill the self-consistency equation for different coupling strengths Ω. The other parameters are $\hbar\delta/J = 2$ and $\hbar\Gamma/J = 1$. For small coupling strengths, the self-consistency equation is only fulfilled at $\lambda = 0$. For higher coupling strengths, a finite value for λ also fulfills the self-consistency equation marking the transition to the self-organized phase.

We now start to analyze the different steady states regarding their dissipative phase transition to self-organized states and how this differs for different system sizes and particle numbers.

One Particle

We begin with the simplest model given by $N = 1$ and $L = 2$. Hence, we only have one symmetry sector spanned by the states with momentum π and 2π and obtain only one steady state solution. Using this solution, we first calculate the cavity occupation as a function of the coupling strength Ω which is depicted in Fig. 6.2.

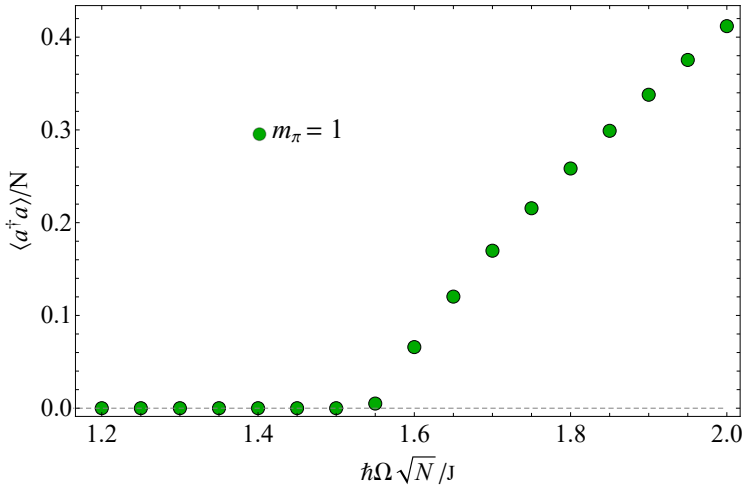

Figure 6.2: Dependence of the scaled photon number $\langle a^\dagger a\rangle/N$ on the scaled coupling strength $\Omega\sqrt{N}$ for $N = 1$ and $L = 2$. The parameters are $\hbar\delta/J = 2$ and $\hbar\Gamma/J = 1$.

For low coupling strengths, the cavity occupation is zero. After passing the critical coupling strength of $\hbar\Omega\sqrt{N}/J \approx 1.5$, the cavity occupation becomes finite and the system is in the self-organized phase.

The transition can be further analyzed by looking at different atomic observables shown in Fig. 6.3. The odd-even imbalance depicted in Fig. 6.3a gets finite in the self-organized phase meaning that the particle occupies the deeper lattice site. Additionally, we find that the off-diagonal terms of the density matrix of the steady state solution, i.e. the coherence, rise in the self-organized phase which is depicted in Fig. 6.3b. Further, we see in Fig. 6.3c that below the phase-transition, the momentum state π corresponding to a lower energy state of the Hamiltonian compared to the state with momentum 2π is mostly occupied, which starts to change above the threshold. In the following, we study how this behavior changes for other steady state solutions in different symmetry sectors by increasing the length L of the atomic chain.

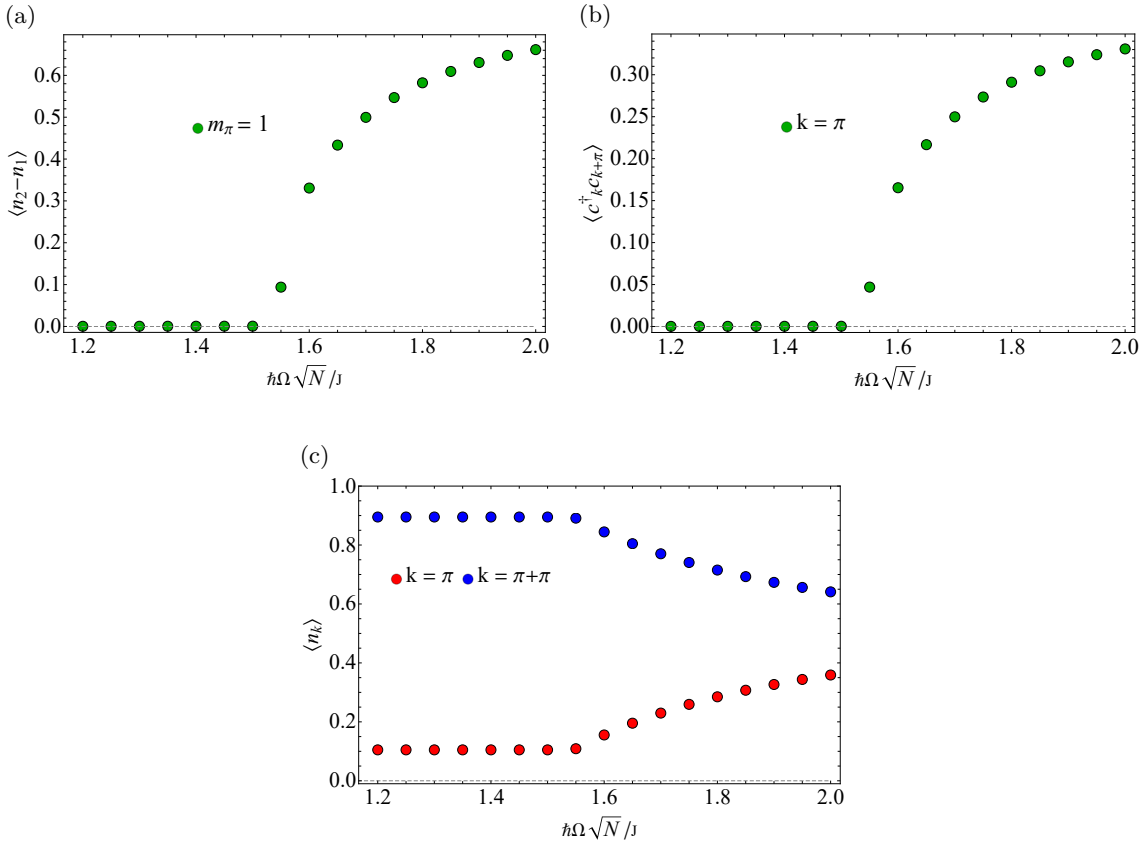

Figure 6.3: (a) shows the dependence of the odd-even imbalance on the scaled coupling strength $\Omega\sqrt{N}$. (b) shows the dependence of the coherence on the scaled coupling strength $\Omega\sqrt{N}$. (c) shows the dependence of the occupation of the possible momenta on the scaled coupling strength $\Omega\sqrt{N}$. All results are for $N = 1$ and $L = 2$ and the parameters are $\hbar\delta/J = 2$ and $\hbar\Gamma/J = 1$.

For $N = 1$ and $L = 4$, we have two symmetry sectors. The first one is spanned by the states with momentum $\pi/2$ and $3\pi/2$ and the second one is spanned by the states with momentum π and 2π. In the first sector $m_{\frac{\pi}{2}} = 1$, we get a two-dimensional solution space instead of one unique steady state. Because of the fact that $\cos(\pi/2) = 0$ and $\cos(3\pi/2) = 0$, the solutions in this sector do not depend on any parameters of the system. Hence, we can write down a general basis of this space which is given by the density matrix

$$\rho = \begin{pmatrix} 1 & 0 \\ 0 & 0 \end{pmatrix}, \tag{6.13}$$

which can be rewritten in momentum space

$$\rho = \begin{pmatrix} u_{\pi/2}^2 & u_{\pi/2}v_{\pi/2} \\ u_{\pi/2}v_{\pi/2} & v_{\pi/2}^2 \end{pmatrix} = \begin{pmatrix} 0.5 & -0.5 \\ -0.5 & 0.5 \end{pmatrix}, \tag{6.14}$$

and by the second density matrix

$$\rho = \begin{pmatrix} 0 & 0 \\ 0 & 1 \end{pmatrix}, \tag{6.15}$$

which can also be rewritten in momentum space

$$\rho = \begin{pmatrix} v_{\pi/2}^2 & -u_{\pi/2}v_{\pi/2} \\ -u_{\pi/2}v_{\pi/2} & u_{\pi/2}^2 \end{pmatrix} = \begin{pmatrix} 0.5 & 0.5 \\ 0.5 & 0.5 \end{pmatrix}, \tag{6.16}$$

where the basis is defined by

$$c_{\pi/2}^\dagger |0\rangle = \begin{pmatrix} 1 \\ 0 \end{pmatrix} \quad \text{and} \quad c_{3\pi/2}^\dagger |0\rangle = \begin{pmatrix} 0 \\ 1 \end{pmatrix}. \tag{6.17}$$

The second sector $m_\pi = 1$ has a unique solution, which leads to the same behavior as in the two site case because the occupied momenta are the same. The cavity occupation as a function of the coupling strength Ω for $N = 1$ and $L = 4$ can be seen in Fig. 6.4.

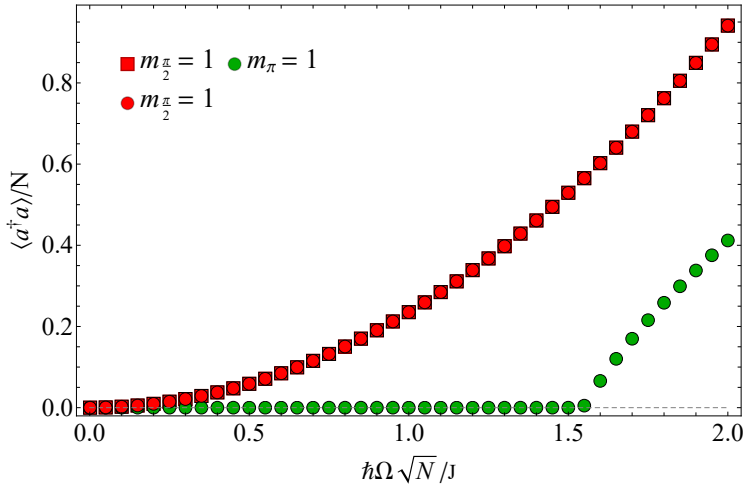

Figure 6.4: Dependence of the scaled photon number $\langle a^\dagger a \rangle / N$ on the scaled coupling strength $\Omega\sqrt{N}$ for $N = 1$ and $L = 4$. The parameters are $\hbar\delta/J = 2$ and $\hbar\Gamma/J = 1$. The solution space in the case $m_{\frac{\pi}{2}} = 1$ is two-dimensional. Hence, a basis of this space consisting of two solutions was used for the phase diagram.

In contrast to the sharp phase transition of the steady state of the second sector $m_\pi = 1$, the solutions of $m_{\frac{\pi}{2}} = 1$ are smooth and show a continuous increase of the cavity occupation by increasing coupling strength.

Again, we have a look at different atomic observables depicted in Fig. 6.5. Since we already discussed the solutions for the symmetry sector $m_{\frac{\pi}{2}} = 1$ explicitly by writing down the density matrices, we do not really gain any new insights there. Additionally, we saw and discussed the behavior of the solution corresponding to the symmetry sector $m_\pi = 1$ already in the two site case. All in all, we see that the steady state solutions of different symmetry sectors can have a very different nature, which in particular influences the phase transition.

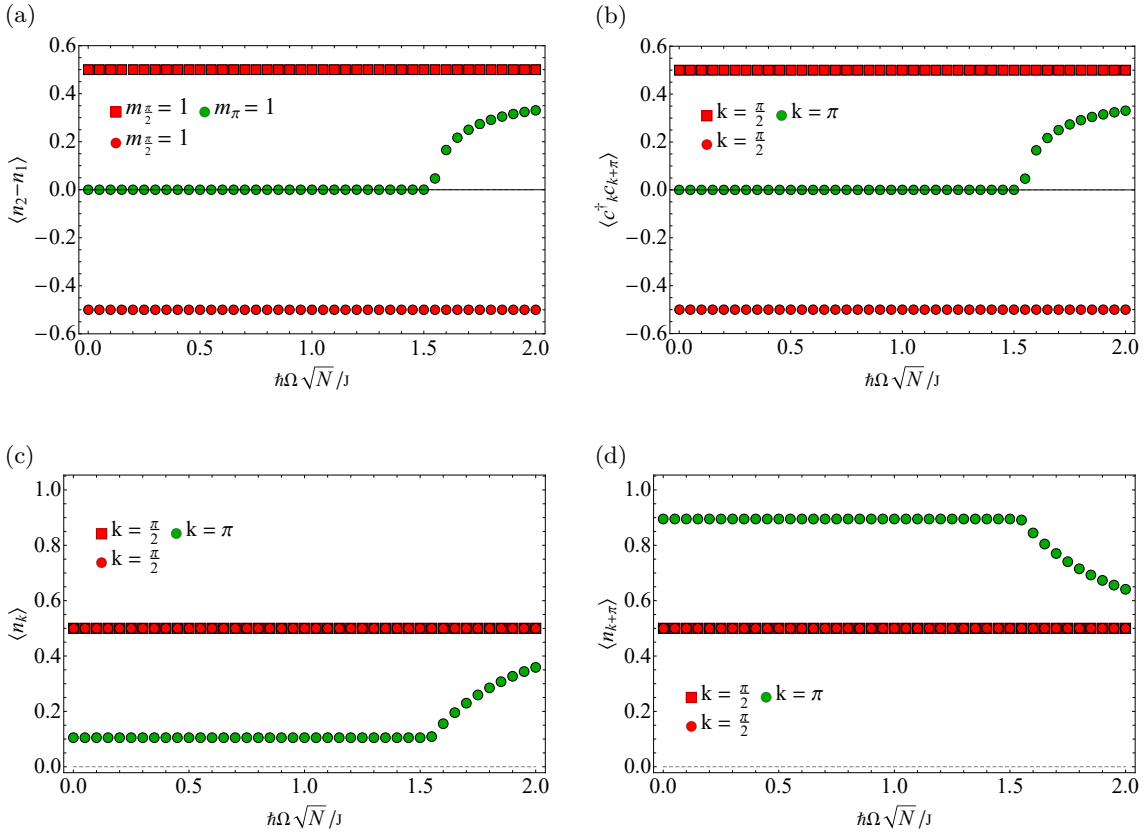

Figure 6.5: (a) shows the dependence of the odd-even imbalance on the scaled coupling strength $\Omega\sqrt{N}$. (b) shows the dependence of the coherence on the scaled coupling strength $\Omega\sqrt{N}$. (c) and (d) show the dependence of the occupation of the possible momenta on the scaled coupling strength $\Omega\sqrt{N}$. All results are for $N = 1$ and $L = 4$ and the parameters are $\hbar\delta/J = 2$ and $\hbar\Gamma/J = 1$.

Next we consider $N = 1$ and $L = 6$. In this case, we have three symmetry sectors. The first one is spanned by the states with momentum $\pi/3$ and $4\pi/3$, the second one is spanned by the states with momentum $2\pi/3$ and $5\pi/3$ and the third one is spanned by the states with momentum π and 2π. Every symmetry sector has a unique steady state. The cavity occupation as a function of the coupling strength Ω can be seen in Fig. 6.6. Again, the steady state solution of the third sector $m_\pi = 1$ is equal to the one in the two site case because the occupied momenta have the same values. The solutions of the other two sectors are matching. The reason for that is that in both of these sectors, we obtain the same eigenenergies of the Hamiltonian because $\cos(\pi/3) = \cos(5\pi/3)$ and $\cos(4\pi/3) = \cos(2\pi/3)$. The critical coupling strength is in this case $\hbar\Omega\sqrt{N}/J \approx 1.2$. In this example of $N = 1$ and $L = 6$, we see in every symmetry sector a sharp increase of the cavity occupation in contrast to the previous situation. However, these transitions differ significantly in their critical coupling strengths. We can explain these different thresholds by looking at the kinetic energy. Since the transition is a competition between the kinetic term and the coupling term, we expect that the threshold depends on the value of the kinetic energy ($\cos(k)$). Thus, the symmetry sector corresponding to a smaller kinetic energy (here $m_{\frac{\pi}{3}} = 1$ and $m_{\frac{2\pi}{3}} = 1$ compared to $m_\pi = 1$) has a smaller transition threshold. Fig. 6.7 shows the corresponding atomic observables. Apart from the difference in the critical coupling strength of the symmetry sectors, a similar behavior can be observed in all sectors. In Fig. 6.11c and 6.11d, it seems that the behavior in the symmetry sector $m_{\pi/3} = 1$ is opposite. But since $\cos(\pi/3 + \pi) > \cos(\pi/3)$, we still observe that below the phase transition the states with a lower energy are mostly occupied in all symmetry sectors.

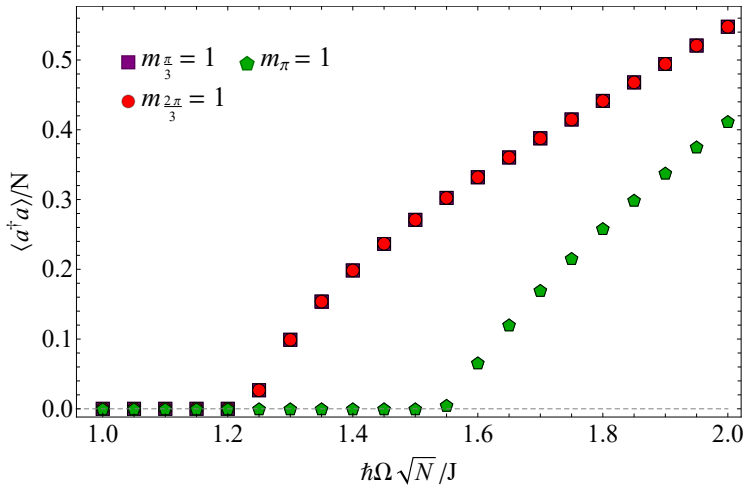

Figure 6.6: Dependence of the scaled photon number $\langle a^\dagger a \rangle / N$ on the scaled coupling strength $\Omega\sqrt{N}$ for $N = 1$ and $L = 6$. The parameters are $\hbar\delta/J = 2$ and $\hbar\Gamma/J = 1$.

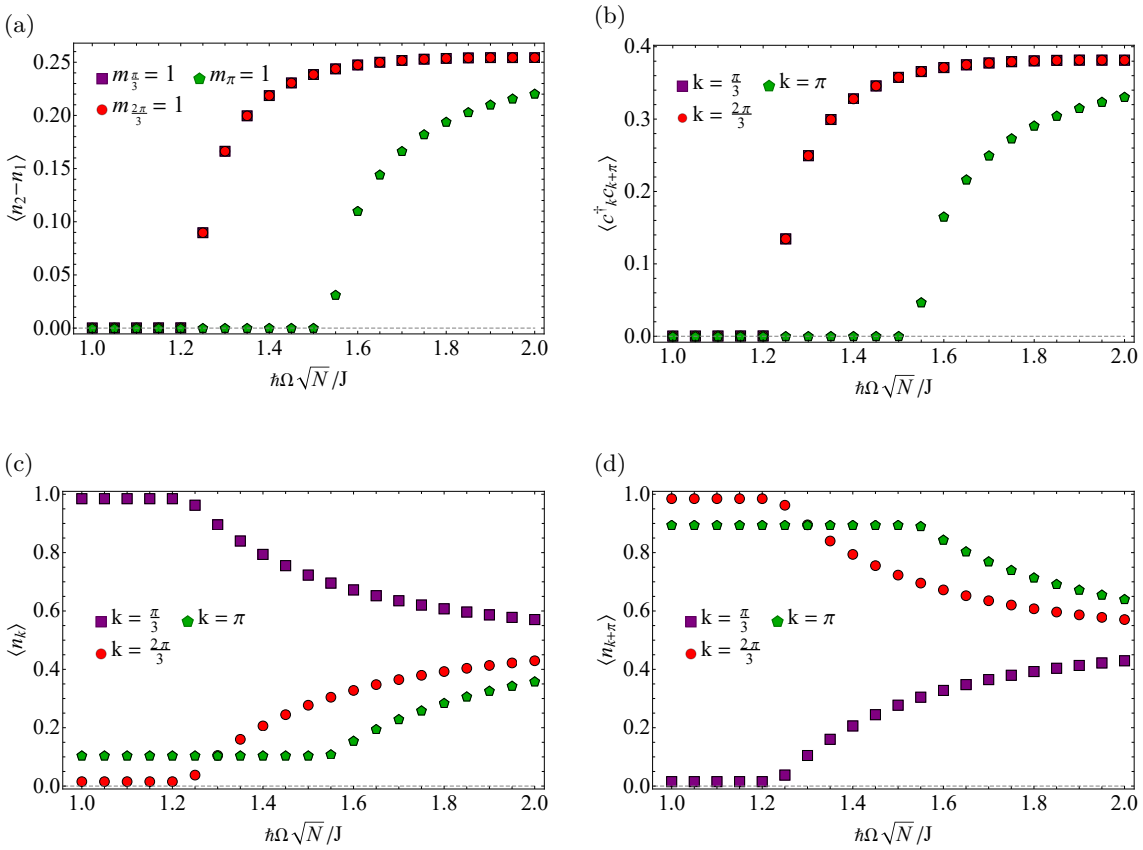

Figure 6.7: (a) shows the dependence of the odd-even imbalance on the scaled coupling strength $\Omega\sqrt{N}$. (b) shows the dependence of the coherence on the scaled coupling strength $\Omega\sqrt{N}$. (c) and (d) show the dependence of the occupation of the possible momenta on the scaled coupling strength $\Omega\sqrt{N}$. All results are for $N = 1$ and $L = 6$ and the parameters are $\hbar\delta/J = 2$ and $\hbar\Gamma/J = 1$.

We go on by considering $N = 1$ and $L = 8$. Here, the four symmetry sectors are spanned by the states with momentum $\pi/4$ and $5\pi/4$, $\pi/2$ and $3\pi/2$, $3\pi/4$ and $7\pi/4$ and π and 2π. For the second

symmetry sector, we observe the same behavior as in the four site case for these momenta. Again, we find the same two-dimensional solution space and use the same basis as before for the following results. All other sectors have a unique steady state. Using these solutions, we calculate the cavity occupation as a function of the coupling strength Ω which is depicted in Fig. 6.8.

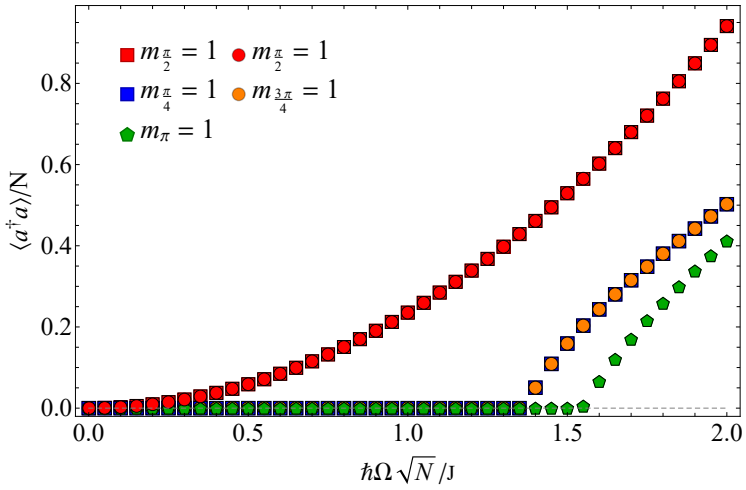

Figure 6.8: Dependence of the scaled photon number $\langle a^\dagger a \rangle / N$ on the scaled coupling strength $\Omega\sqrt{N}$ for $N = 1$ and $L = 8$. The parameters are $\hbar\delta/J = 2$ and $\hbar\Gamma/J = 1$. The solution space in the case $m_{\frac{\pi}{2}} = 1$ is two dimensional. Hence, a basis of this space consisting of two solutions was used for the phase diagram.

New in this particular case are the symmetry sector $m_{\pi/4} = 1$ and the symmetry sector $m_{3\pi/4} = 1$ leading to another critical coupling strength of $\hbar\Omega\sqrt{N}/J \approx 1.35$. Both sectors lead to the same critical coupling strength and are further completely matching because we obtain the same eigenenergies of the Hamiltonian for both. We have already seen this in the case of $N = 1$ and $L = 6$ for the sectors $m_{\pi/3} = 1$ and $m_{2\pi/3} = 1$. The corresponding atomic observables can be seen in Fig. 6.9. Again, we discussed most of the symmetry sectors already previously and the general features of the solutions of the symmetry sector $m_{\pi/4} = 1$ and the symmetry sector $m_{3\pi/4} = 1$ are apart from the different critical coupling strength very similar.

As a last example in the single particle case, we have a look at $N = 1$ and $L = 10$, where the five symmetry sectors are spanned by the states with momentum $\pi/5$ and $6\pi/5$, $2\pi/5$ and $7\pi/5$, $3\pi/5$ and $8\pi/5$, $4\pi/5$ and $9\pi/5$ and π and 2π. All of these sectors have a unique steady state. The cavity occupation as a function of the coupling strength Ω can be seen in Fig. 6.10. Except for the symmtery sector $m_\pi = 1$, all of the momenta of the other symmetry sectors were not present in the examples discussed so far. The steady state of the symmetry sector $m_{\pi/5} = 1$ leads to the critical coupling strength of $\hbar\Omega\sqrt{N}/J \approx 1.4$ as well as the steady state of the symmetry sector $m_{4\pi/5} = 1$. Furthermore, the steady state of the symmetry sector $m_{2\pi/5} = 1$ leads to the critical coupling strength of $\hbar\Omega\sqrt{N}/J \approx 1.1$ as well as the steady state of the symmetry sector $m_{3\pi/5} = 1$. The same behavior in these symmetry sectors is again due to the fact that the states have the same eigenenergies of the Hamiltonian. By looking at some atomic obervables depicted in Fig. 6.11 we do not see any new special features apart from the different critical coupling strengths in the different symmetry sectors.

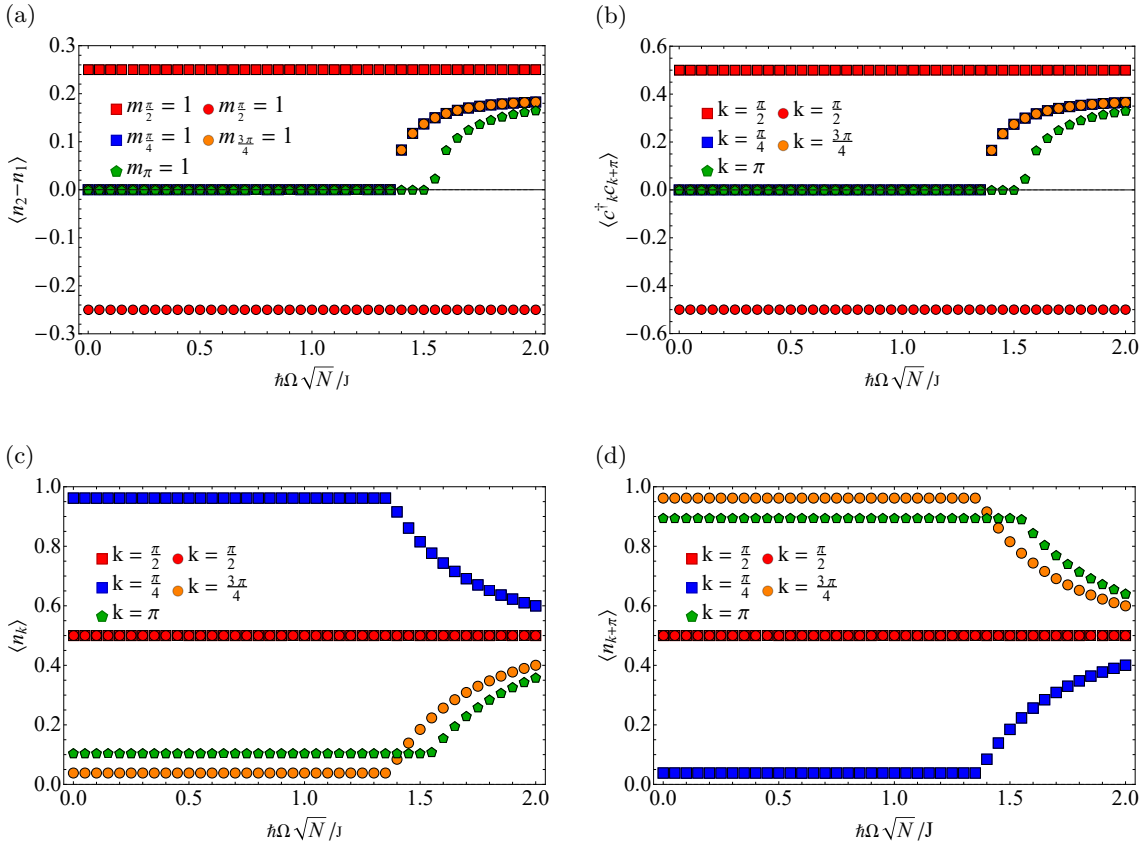

Figure 6.9: (a) shows the dependence of the odd-even imbalance on the scaled coupling strength $\Omega\sqrt{N}$. (b) shows the dependence of the coherence on the scaled coupling strength $\Omega\sqrt{N}$. (c) and (d) show the dependence of the occupation of the possible momenta on the scaled coupling strength $\Omega\sqrt{N}$. All results are for $N = 1$ and $L = 8$ and the parameters are $\hbar\delta/J = 2$ and $\hbar\Gamma/J = 1$.

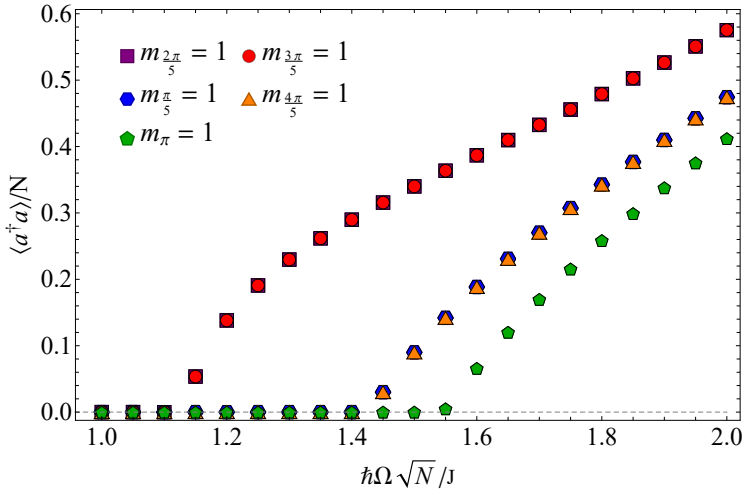

Figure 6.10: Dependence of the scaled photon number $\langle a^\dagger a \rangle / N$ on the scaled coupling strength $\Omega\sqrt{N}$ for $N = 1$ and $L = 10$. The parameters are $\hbar\delta/J = 2$ and $\hbar\Gamma/J = 1$.

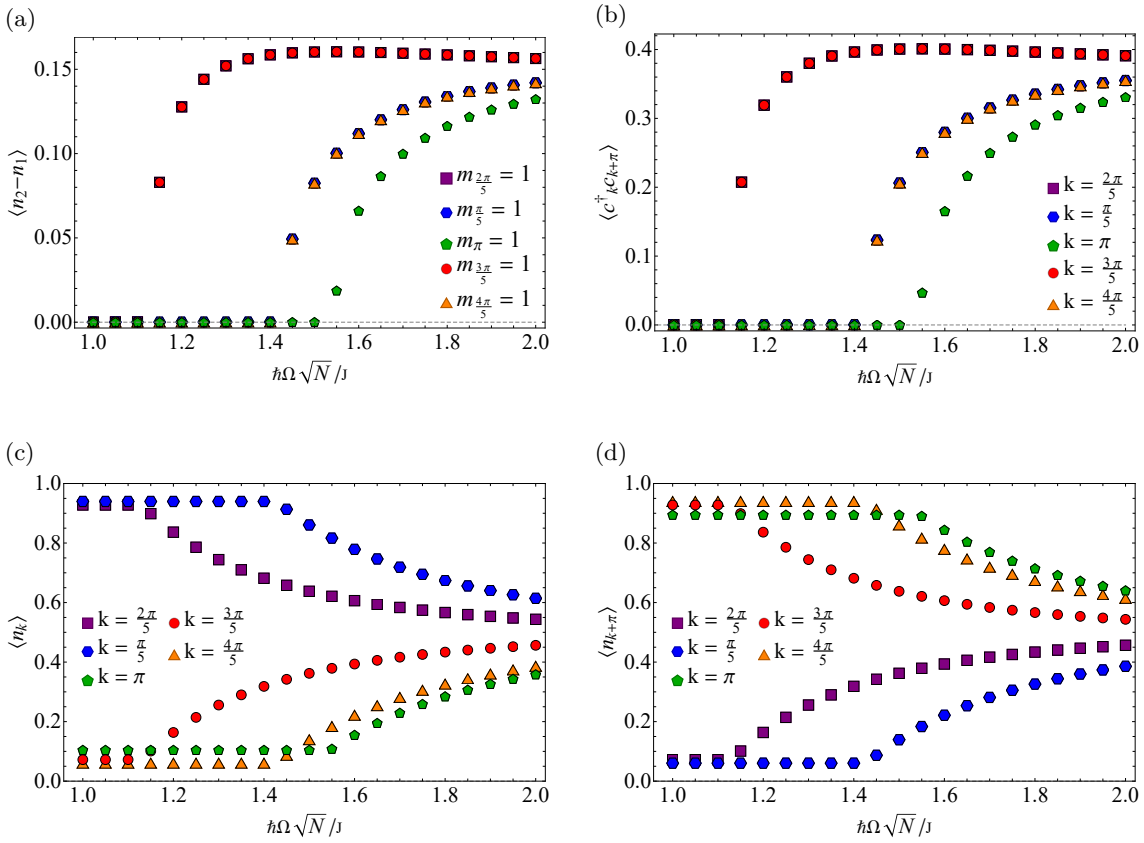

Figure 6.11: (a) shows the dependence of the odd-even imbalance on the scaled coupling strength $\Omega\sqrt{N}$. (b) shows the dependence of the coherence on the scaled coupling strength $\Omega\sqrt{N}$. (c) and (d) show the dependence of the occupation of the possible momenta on the scaled coupling strength $\Omega\sqrt{N}$. All results are for $N = 1$ and $L = 10$ and the parameters are $\hbar\delta/J = 2$ and $\hbar\Gamma/J = 1$.

Two Particles

We now start to increase the particle number and consider $N = 2$ and $L = 4$. This situation offers two possibilities. We can either put both particles in one of the single particle symmetry sectors or we put one particle in the first sector and the other one in the second sector. If we put both of these particles in the same single particle sector, we expect no dynamics to occur. In the other situation, we get a two-dimensional solution space. The cavity occupation as a function of the coupling strength Ω can be seen in Fig. 6.12. One sees that the cavity occupation stays zero in the case where both particles are in the same single particle sector, i.e. either $m_{\frac{\pi}{2}} = 2$ or $m_\pi = 2$. We can also show analytically that a completely filled symmetry sector does not contribute to the dynamics in our system, i.e. to the cavity occupation. The occupation of the cavity is given by

$$\langle a^\dagger a \rangle = \frac{\Omega^2}{\delta^2 + \Gamma^2/4} \operatorname{Tr}(\rho\, O)^2, \tag{6.18}$$

with the imbalance operator $O = \sum_k c_k^\dagger c_{k+\pi}$. Now we consider the situation that we have two particles which occupy the same single particle symmetry sector spanned by the states with momentum p and $p + \pi$. The density matrix can then be written as $\rho = c^\dagger_{p+\pi} c^\dagger_p A^\dagger |0\rangle \langle 0| A c_p c_{p+\pi}$, where $A^\dagger$ contains linear combinations of products of creation operators associated with the other symmetry sectors. In particular, $A^\dagger$ does not contain the operators $c^\dagger_p$ and $c^\dagger_{p+\pi}$. We then find for

the trace

$$\begin{aligned}
&\mathrm{Tr}(c_{p+\pi}^\dagger c_p^\dagger A^\dagger \left|0\right\rangle \left\langle 0\right| A c_p c_{p+\pi} \sum_k c_k^\dagger c_{k+\pi}) \\
=&\sum_k \mathrm{Tr}(c_{p+\pi}^\dagger c_p^\dagger A^\dagger \left|0\right\rangle \left\langle 0\right| A\{c_p c_{p+\pi}, c_k^\dagger c_{k+\pi}\}) - \sum_k \mathrm{Tr}(c_{p+\pi}^\dagger c_p^\dagger A^\dagger \left|0\right\rangle \left\langle 0\right| A c_k^\dagger c_{k+\pi} c_p c_{p+\pi}) \\
=&\sum_k \mathrm{Tr}(c_{p+\pi}^\dagger c_p^\dagger A^\dagger \left|0\right\rangle \left\langle 0\right| A(\delta_{p+\pi,k} c_p c_{k+\pi} - \delta_{p,k} c_{p+\pi} c_{k+\pi} + 2c_k^\dagger c_{k+\pi} c_p c_{p+\pi})) \\
&- \sum_k \mathrm{Tr}(c_{p+\pi}^\dagger c_p^\dagger A^\dagger \left|0\right\rangle \left\langle 0\right| A c_k^\dagger c_{k+\pi} c_p c_{p+\pi}) \\
=&\sum_k \mathrm{Tr}(c_{p+\pi}^\dagger c_p^\dagger A^\dagger \left|0\right\rangle \left\langle 0\right| A c_k^\dagger c_{k+\pi} c_p c_{p+\pi}) \\
=&\sum_k \mathrm{Tr}(A^\dagger \left|0\right\rangle \left\langle 0\right| A c_k^\dagger c_{k+\pi}),
\end{aligned} \tag{6.19}$$

where the trace in the last line stands for the trace over the $(N-2)$-particle states. Therefore, a completely filled symmetry sector does not contribute to the cavity occupation. Hence, we will not further analyze the two cases of $m_{\frac{\pi}{2}} = 2$ and $m_\pi = 2$. In the situation $m_{\frac{\pi}{2}} = m_\pi = 1$, one of the two solutions looks similar to the solutions which we have seen in the single particle case for the symmetry sector $m_{\frac{\pi}{2}} = 1$. For the other solution, we find a very quick saturation of the increasing photon number which then starts to decrease. To get a better understanding for that we look at some atomic observables depicted in Fig. 6.13. In Fig. 6.13a, we see that the odd-even imbalance tends to go to zero for the solution which showed only a weak increase followed by a decrease in the photon number. In Fig. 6.13b, Fig. 6.13c and Fig. 6.13d, we encounter for the momentum $\pi/2$ the same behavior as in the single particle case for this momentum. Hence, the interplay between the two involved single particle symmetry sectors leads to the observed behavior.

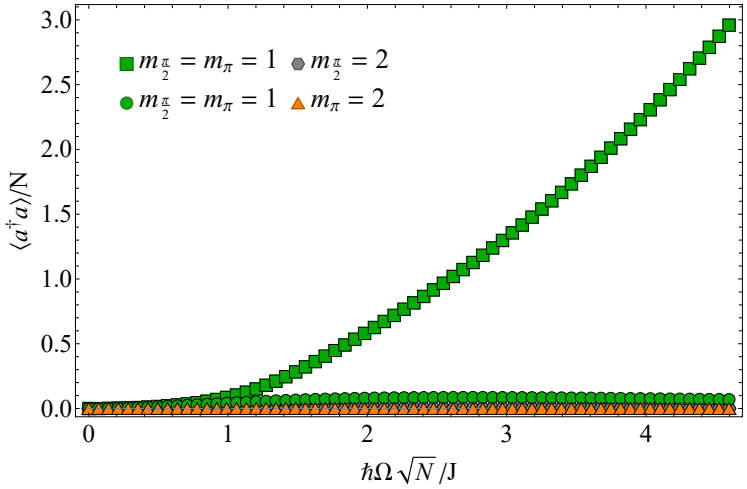

Figure 6.12: Dependence of the scaled photon number $\langle a^\dagger a\rangle/N$ on the scaled coupling strength $\Omega\sqrt{N}$ for $N = 2$ and $L = 4$. The parameters are $\hbar\delta/J = 2$ and $\hbar\Gamma/J = 1$. The solution space in the case $m_{\frac{\pi}{2}} = m_\pi = 1$ is two-dimensional. Hence, a basis of this space consisting of two solutions was used for the phase diagram.

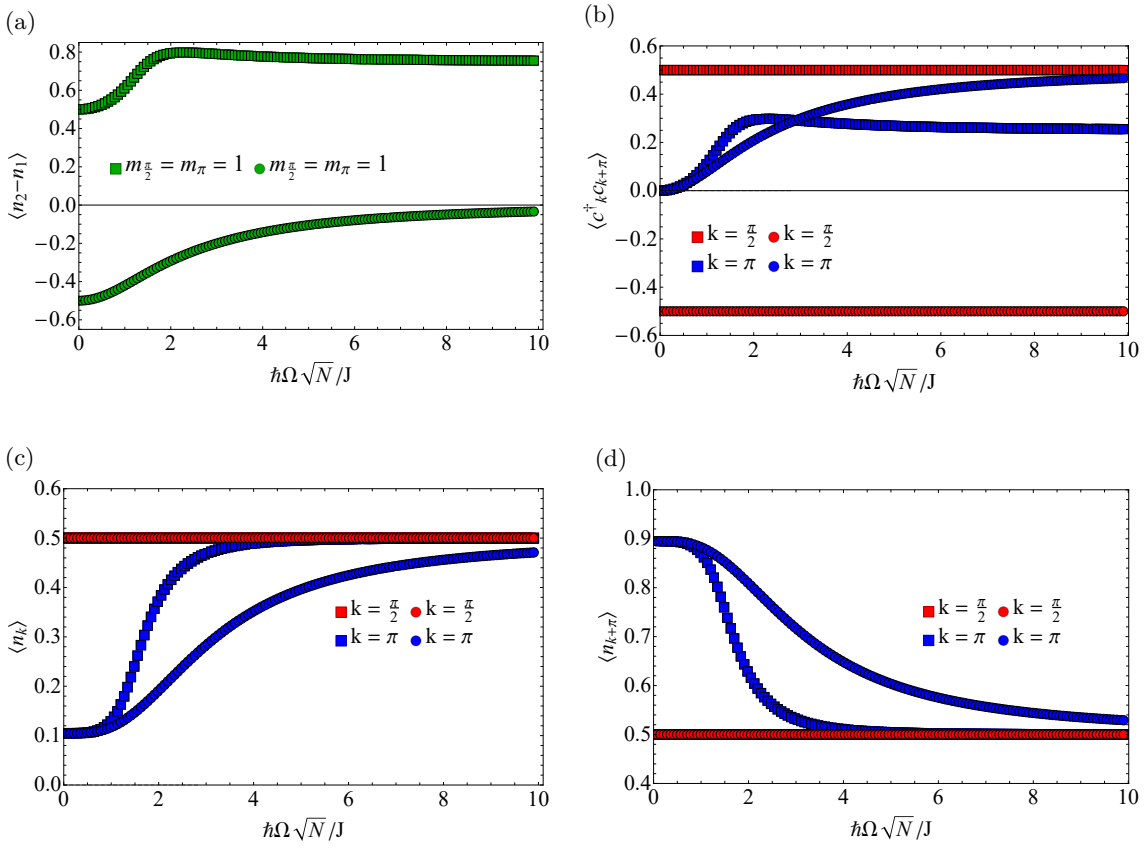

Figure 6.13: (a) shows the dependence of the odd-even imbalance on the scaled coupling strength $\Omega\sqrt{N}$. (b) shows the dependence of the coherence on the scaled coupling strength $\Omega\sqrt{N}$. (c) and (d) show the dependence of the occupation of the possible momenta on the scaled coupling strength $\Omega\sqrt{N}$. All results are for $N = 2$ and $L = 4$ and the parameters are $\hbar\delta/J = 2$ and $\hbar\Gamma/J = 1$. Note that we use the notation that the squares correspond to one solution and the circles to the other one.

Three Particles

Next we increase the particle number further and consider $N = 3$ and $L = 6$. Here, we have six different combinations of filling one symmetry sector completely with two particles and having the other particle in one of the two remaining sectors. Moreover, we can put one particle in every single particle symmetry sector. Referring to our previous analysis, the completely filled symmetry sectors do not contribute to the cavity occupation. Hence, we expect that we get the same dynamics as in the case for $N = 1$ and $L = 6$. Fig. 6.14 shows the the cavity occupation as a function of the coupling strength Ω for all six possible combinations. One sees that the completely filled single particle sector does not contribute to the result as the occupation of one of the single particle sectors does not change by the choice of the completely filled sector. Furthermore, the results are the same as in the one particle case for six sites up to rescaling with the particle number, which were shown in Fig. 6.6.

If we put one particle in every single particle symmetry sector, we get a two-dimensional solution space, because two of the single particle sectors have the same energy and in this case both are occupied simultaneously.

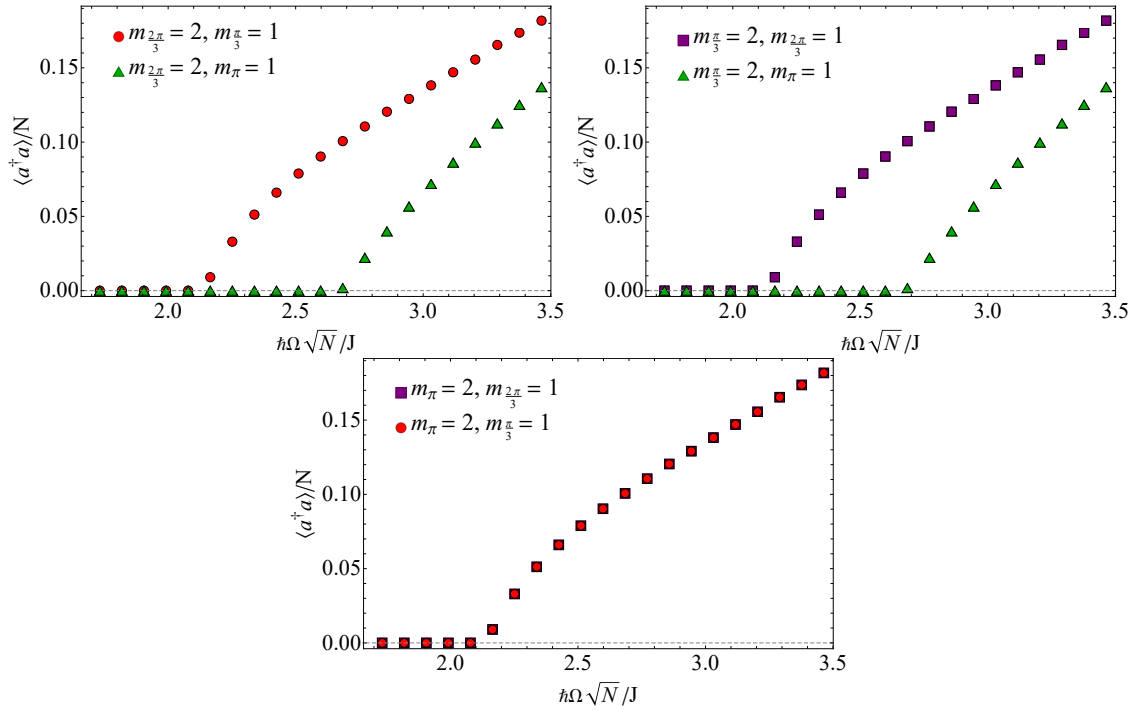

Figure 6.14: Dependence of the scaled photon number $\langle a^\dagger a\rangle/N$ on the scaled coupling strength $\Omega\sqrt{N}$ for $N = 3$ and $L = 6$. The parameters are $\hbar\delta/J = 2$ and $\hbar\Gamma/J = 1$.

Four Particles

As a last example of this analysis, we want to comment on the system with $N = 4$ and $L = 8$. Here, we have 19 different subspaces for which we want to find the steady states. Six subspaces cover the situation where two single particle sectors are completely filled, 12 of them capture that one single particle sector is completely filled and in the last subspace every particle is in one of the single particle symmetry sectors. The latter leads to a four-dimensional solution space because of the fact that two of the single particle sectors have the same energy (the ones spanned by the states with momentum $\pi/4$ and $5\pi/4$ and with momentum $3\pi/4$ and $7\pi/4$) and the $\pi/2$ sector is also occupied. Depending on which one particle sector is entirely filled and which single particle sectors are occupied by the remaining two particles, the solution space is either one or two-dimensional. If two single particle sectors are totally filled, the solution space is one-dimensional and as shown before, the cavity occupation stays zero.

For larger systems especially regarding the number of atoms, it becomes computationally more difficult to find the steady state solutions since we are solving for every entry of the density matrix separately. Therefore, we focus on the interacting model in the next chapter, where we can use a thermal ansatz to describe the atomic part of the density matrix which reduces the degrees of freedom in our computation significantly. There, we will also compare the results obtained within the mean-field approach without any fluctuations with the one of the many-body adiabatic elimination. The goal here was to understand the influence of a strong symmetry of the Liouvillian on the nature of the steady state solutions. We have seen that we obtain multiple steady state solutions for which the resulting phase transitions differ in their critical coupling strength or do not show a sharp phase transition at all. These different thresholds imply a coexistence of states of different natures for the same parameters depending on the chosen symmetry sector.

7 The interacting system

In this chapter, we study the self-organization transition for the full model introduced in Chapter 3 in Eq. 3.9. For this, we use the steady state solutions obtained by using the ground state of the effective mean-field Hamiltonian (see Eq. 4.8) as well as the ones from the many-body adiabatic elimination (see Eq. 4.30). For the latter, we describe the atomic part of the density matrix by a thermal state and solve for the effective temperature in contrast to the situation discussed previously in the non-interacting limit of the model. As we have seen there, symmetries play a crucial role in the analysis of the steady state solutions and the resulting phase transition. In the interacting system, we can find again strong symmetries of the Liouvillian, i.e. a translation symmetry and a reflection symmetry, if we assume periodic boundary conditions for our atomic chain. In contrast, these symmetries are not present for open boundary conditions. We will discuss both cases in the following. In the analysis, we restrict to a fixed particle number N and we fix $S_z = 0$. It is important to note that we showed the non-integrability of the ionic Hubbard model in Chapter 5, which we need for the applicability of the thermal ansatz for the atomic part of the density matrix. But this is only valid as soon as the cavity is occupied. We will nevertheless also use this ansatz below the phase transition for our results. However, the behavior in this regime would actually have to be investigated separately.

7.1 Steady state solutions for open boundary conditions

We start by using open boundary conditions for the atomic chain. In order to investigate the behavior of the system across the self-organization transition, we have a look at the occupation of the cavity $\langle a^\dagger a\rangle$ and at the contrast in the density-density correlations

$$\frac{1}{L-2}\sum_{i=1}^{L-2}(\langle n_i n_{i+2}\rangle - \langle n_i n_{i+1}\rangle) \quad \text{with} \quad n_i = \sum_\sigma n_{i,\sigma}. \tag{7.1}$$

The latter is the measure of the density wave character. Further, we calculate these observables by either varying the coupling strength Ω for a fixed dissipation strength Γ or by varying the dissipation strength Γ for a fixed coupling strength Ω.

For quarter-filling, i.e $N = 2$ and $L = 4$, Fig. 7.1 depicts the results obtained by using the ground state of the effective mean-field Hamiltonian. In Sec. 4.1, we already discussed the behavior of the cavity field within this approach taking a finite value in the self-organized phase. This can be seen in Fig. 7.1a. Additionally, we now see in Fig. 7.1c that the atoms self-organize into a density modulated pattern either on the odd or even sites of the chain. The contrast takes the value $1/2$ in the self-organized phase showing that within this mean-field approach the atomic state approaches a total population imbalance where no defects are present. In Fig. 7.1b and 7.1d, we can observe a transition back into the normal phase by increasing the dissipation strength in the system.

We can compare these results with the ones obtained within the many-body adiabatic elimination. Thus, we can see how the fluctuations change the previously seen behavior. Starting with Fig. 7.2a and Fig. 7.2c for low Γ, we see that the position of the phase transition does not really change ($\hbar\Omega\sqrt{N}/J \approx 1.35$) but we encounter a small jump at the phase transition in the photon number and in the contrast, which was not present in the mean-field results. Further, we see that the fluctuations lead to a significant decrease of the amount of photons inside the cavity which even starts to saturate for higher coupling strengths Ω. This effect is also visible in the contrast which clearly shows the different nature of our atomic state compared to the pure state within the mean-field approach without fluctuations. The fluctuations lead to a mixed state including states without a total population imbalance, which significantly reduces the contrast. We also see

that the contrast starts to decreases as we go to larger Ω in the self-organized phase. This can be explained by looking at the inverse temperature $\beta = 1/k_B T$ depicted in Fig. 7.2e. The temperature increases strongly in the self-organized phase and is also finite below the transition threshold due to the fluctuations. This is in contrast to the mean-field solution without fluctuation which is a zero temperature state. The temperature further leads to excitations in the atomic sector which explains the decreasing contrast and also the suppressed photon number.

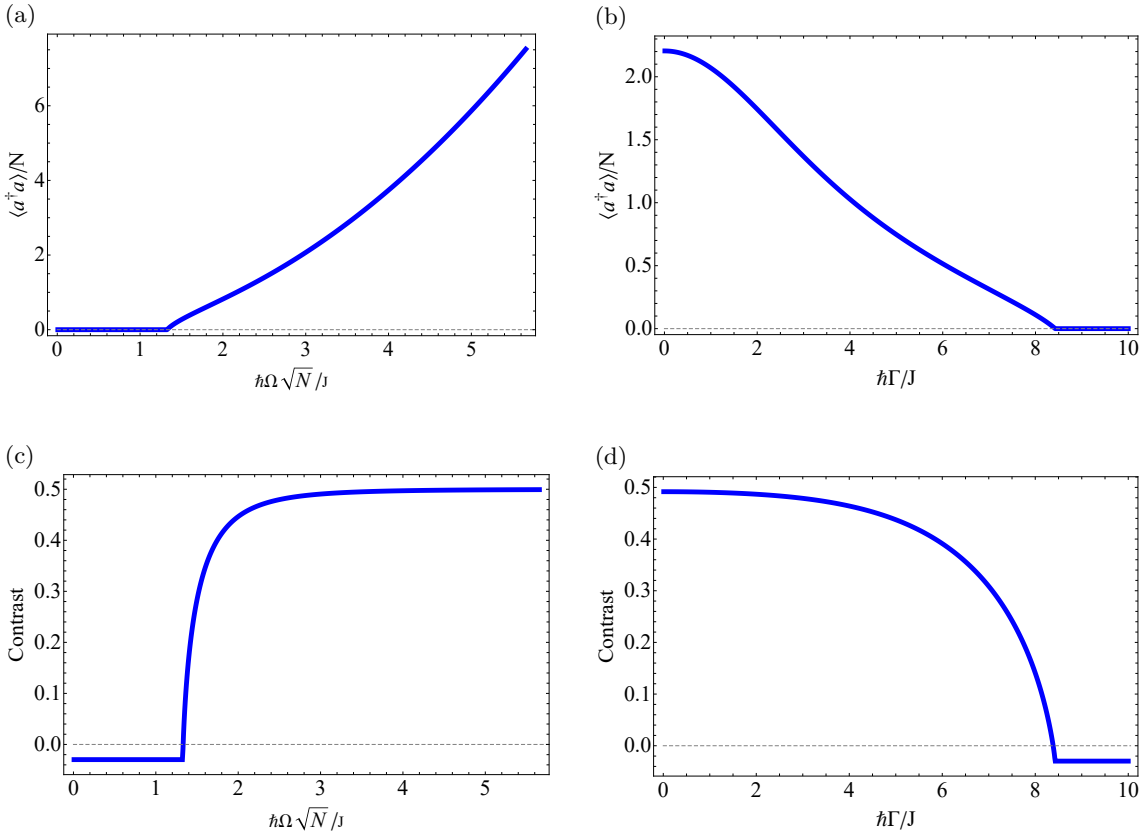

Figure 7.1: Results of the zero temperature mean-field approach. (a) and (c) show the dependence of the scaled photon number $\langle a^\dagger a \rangle / N$ and of the contrast on the scaled coupling strength $\Omega\sqrt{N}$ for $N = 2$ and $L = 4$. The parameters are $\hbar\delta/J = 2$, $U/J = 2$ and $\hbar\Gamma/J = 1$. (b) and (d) show the dependence of the scaled photon number $\langle a^\dagger a \rangle / N$ and of the contrast on the dissipation strength Γ for $N = 2$ and $L = 4$. The parameters are $\hbar\delta/J = 2$, $U/J = 2$ and $\hbar\Omega\sqrt{N}/J = 3$.

Switching to the situation where we observe the transition back into the normal phase as we increase Γ in Fig. 7.2b, Fig. 7.2d and Fig. 7.2e, we first see that we do not see a jump at the transition point in all observables. Moreover, we obtain in this regime of strong dissipation a very different transition threshold ($\hbar\Gamma/J \approx 5.6$) compared to the zero temperature mean-field solution ($\hbar\Gamma/J \approx 8.4$). We expected this significant deviation for strong dissipation stengths referring to the analysis done for an analogous model for bosonic atoms by Bezvershenko et al. [11] and Halati [13]. Apart from that, we find a very similar behavior to the situation before, as the photon number and contrast are much below the ones from the zero temperature mean-field solution.

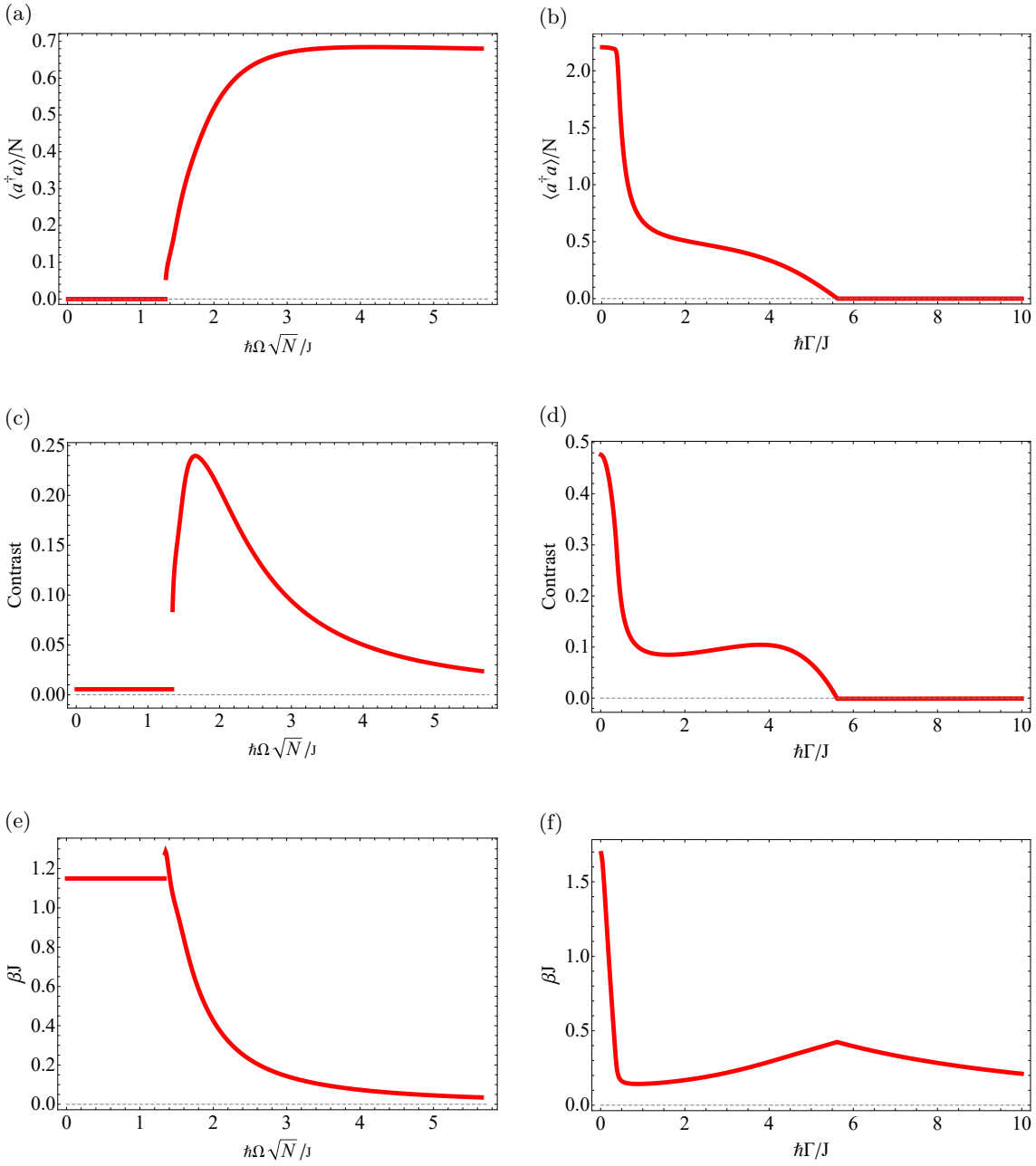

Figure 7.2: Results of the finite temperature many-body adiabatic elimination approach. (a), (c) and (e) show the dependence of the scaled photon number $\langle a^\dagger a\rangle/N$, of the contrast and of the inverse temperature β on the scaled coupling strength $\Omega\sqrt{N}$ for $N = 2$ and $L = 4$. The parameters are $\hbar\delta/J = 2$, $U/J = 2$ and $\hbar\Gamma/J = 1$. (b), (d) and (f) show the dependence of the scaled photon number $\langle a^\dagger a\rangle/N$, of the contrast and of the inverse temperature β on the dissipation strength Γ for $N = 2$ and $L = 4$. The parameters are $\hbar\delta/J = 2$, $U/J = 2$ and $\hbar\Omega\sqrt{N}/J = 3$.

As a second example, we have a look at a half-filled chain, i.e. $N = 4$ and $L = 4$. Again, we first consider the zero temperature mean-field solution shown in Fig. 7.3.

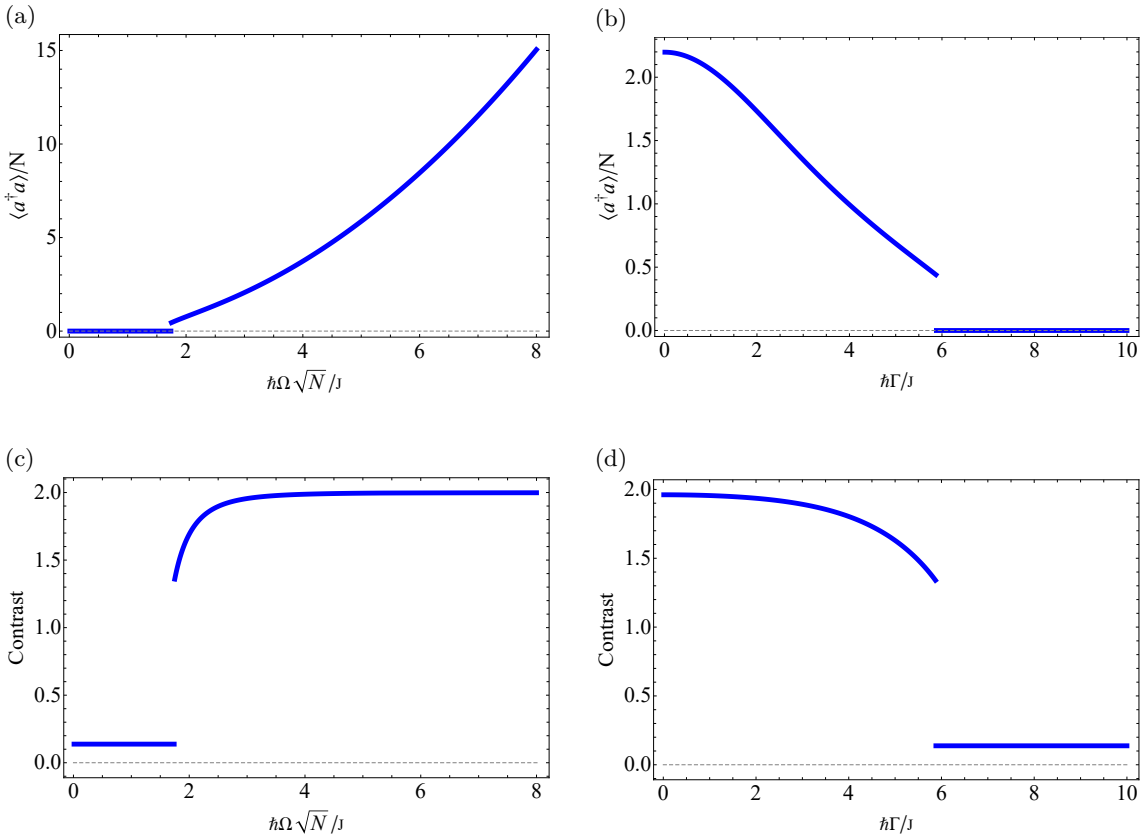

Figure 7.3: Results of the zero temperature mean-field approach. (a) and (c) show the dependence of the scaled photon number $\langle a^\dagger a\rangle/N$ and of the contrast on the scaled coupling strength $\Omega\sqrt{N}$ for $N = 4$ and $L = 4$. The parameters are $\hbar\delta/J = 2$, $U/J = 2$ and $\hbar\Gamma/J = 1$. (b) and (d) show the dependence of the scaled photon number $\langle a^\dagger a\rangle/N$ and of the contrast on the dissipation strength Γ for $N = 4$ and $L = 4$. The parameters are $\hbar\delta/J = 2$, $U/J = 2$ and $\hbar\Omega\sqrt{N}/J = 3$.

Here we observe a jump at the transition point in all cases. Compared to the quarter-filled case, the transition point is now at a higher coupling strength $\hbar\Omega\sqrt{N}/J \approx 1.75$ and at a lower dissipation strength $\hbar\Gamma/J \approx 5.8$. Apart from that, we do not observe any new features here.

Comparing this to the results of the mean-field solution including the fluctuations reveals the same major differences as we have already seen in the case of quarter-filling. Due to the strong increase of the effective temperature (see Fig. 7.4e), the photon number (see Fig. 7.4a) and the contrast (see Fig. 7.4c) are significantly suppressed but the transition threshold again does not really deviate from the zero temperature mean-field solution at low Γ. Furthermore, the jump at the transition point is now even more pronounced compared to the case of quarter-filling (see Fig. 7.2a and Fig. 7.2c). However, the jump disappears at the transition back into the normal phase shown as a function of Γ in Fig. 7.4b, Fig. 7.4d and Fig. 7.4f. In this regime of strong dissipation strengths, the deviation of the transition threshold ($\hbar\Gamma/J \approx 4.2$) to the zero temperature mean-field solution ($\hbar\Gamma/J \approx 5.8$) is substantial as we have also seen in the case of quarter-filling.

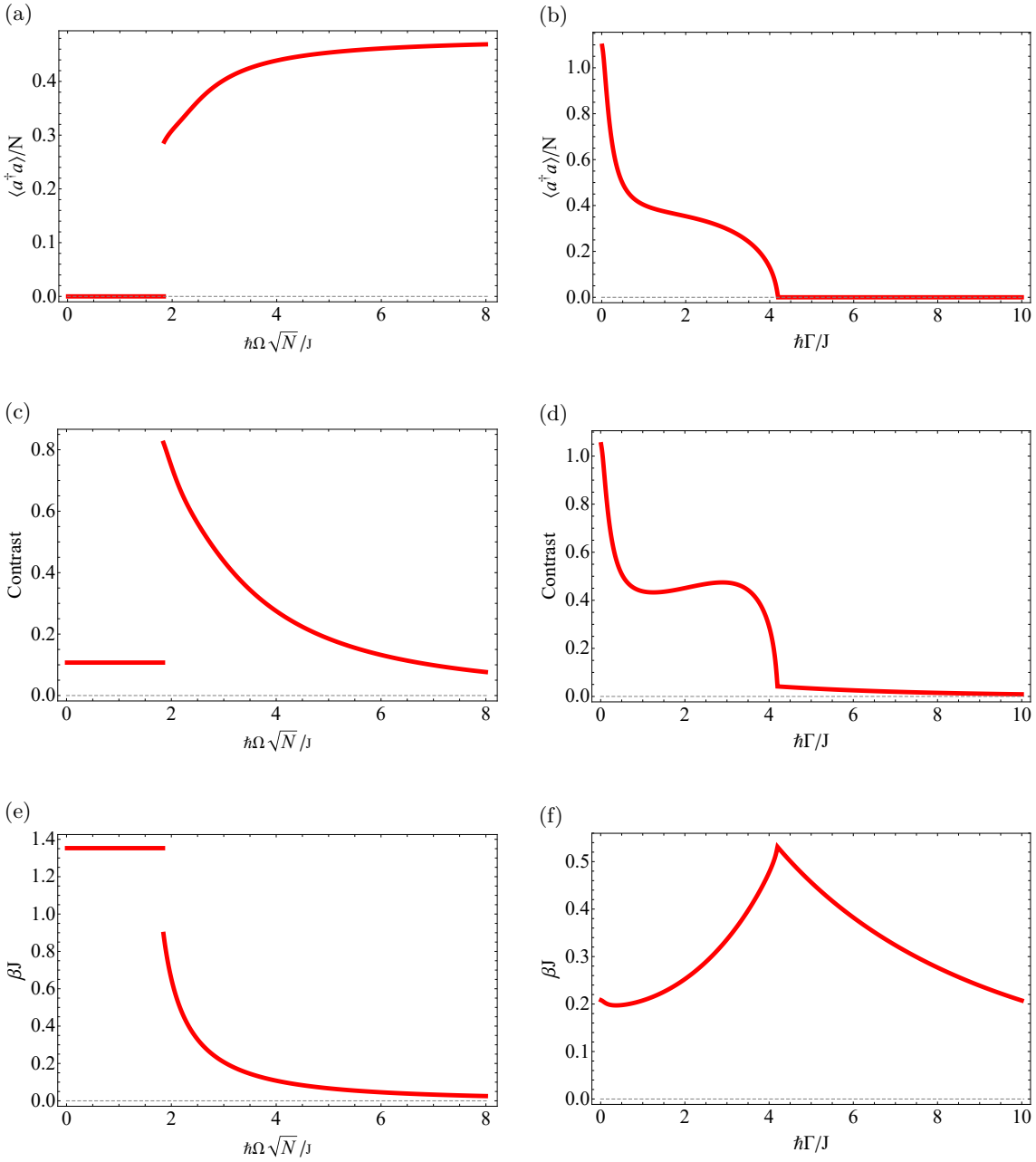

Figure 7.4: Results of the finite temperature many-body adiabatic elimination approach. (a), (c) and (e) show the dependence of the scaled photon number $\langle a^\dagger a\rangle/N$, of the contrast and of the inverse temperature β on the scaled coupling strength $\Omega\sqrt{N}$ for $N = 4$ and $L = 4$. The parameters are $\hbar\delta/J = 2$, $U/J = 2$ and $\hbar\Gamma/J = 1$. (b), (d) and (f) show the dependence of the scaled photon number $\langle a^\dagger a\rangle/N$, of the contrast and of the inverse temperature β on the dissipation strength Γ for $N = 4$ and $L = 4$. The parameters are $\hbar\delta/J = 2$, $U/J = 2$ and $\hbar\Omega\sqrt{N}/J = 3$.

All in all, we have seen that the influence of fluctuations onto the nature of our states is enormous. Fluctuations lead to a finite temperature mixed atomic state in the self-organized phase meaning that states without a total population imbalance do also contribute to our steady state. This was in particular visible in the suppressed photon number inside the cavity and the saturation of it and also in the smaller contrast and the decrease of it.

7.2 Steady state solutions for periodic boundary conditions

The strong symmetries which are now present for periodic boundary conditions, where already mentioned in Sec. 5.1. There we saw that the atomic mean-field Hamiltonian has a translation symmetry and a reflection symmetry. Since the transformations associated to these symmetries only act on the fermionic operators, it is straightforward to show that these commute with the annihilation operator a and thus also with the coupling term H_{ac} without performing the mean-field decoupling. Therefore, these two spatial symmetries are strong symmetries of the Liouvillian and we analyze the steady state solution in every of the resulting symmetry sectors[1]. The labeling of these sectors will be the same as introduced in Sec. 5.1. For $L = 4$, we have four different symmetry sectors. The translation symmetry leads to a splitting into two symmetry sectors which we label by $k = 0$ and $k = 1$. The reflection symmetry leads to a further splitting of each of these blocks into two more symmetry sectors labeled by $+$ and $-$. Thus, all together we have four different symmetry sectors, which we label by $(0,-)$, $(0,+)$, $(1,-)$ and $(1,+)$.

We start with a quarter-filled atomic chain, i.e. $N = 2$ and $L = 4$. Fig. 7.5 shows the results obtained by using the zero temperature mean-field state.

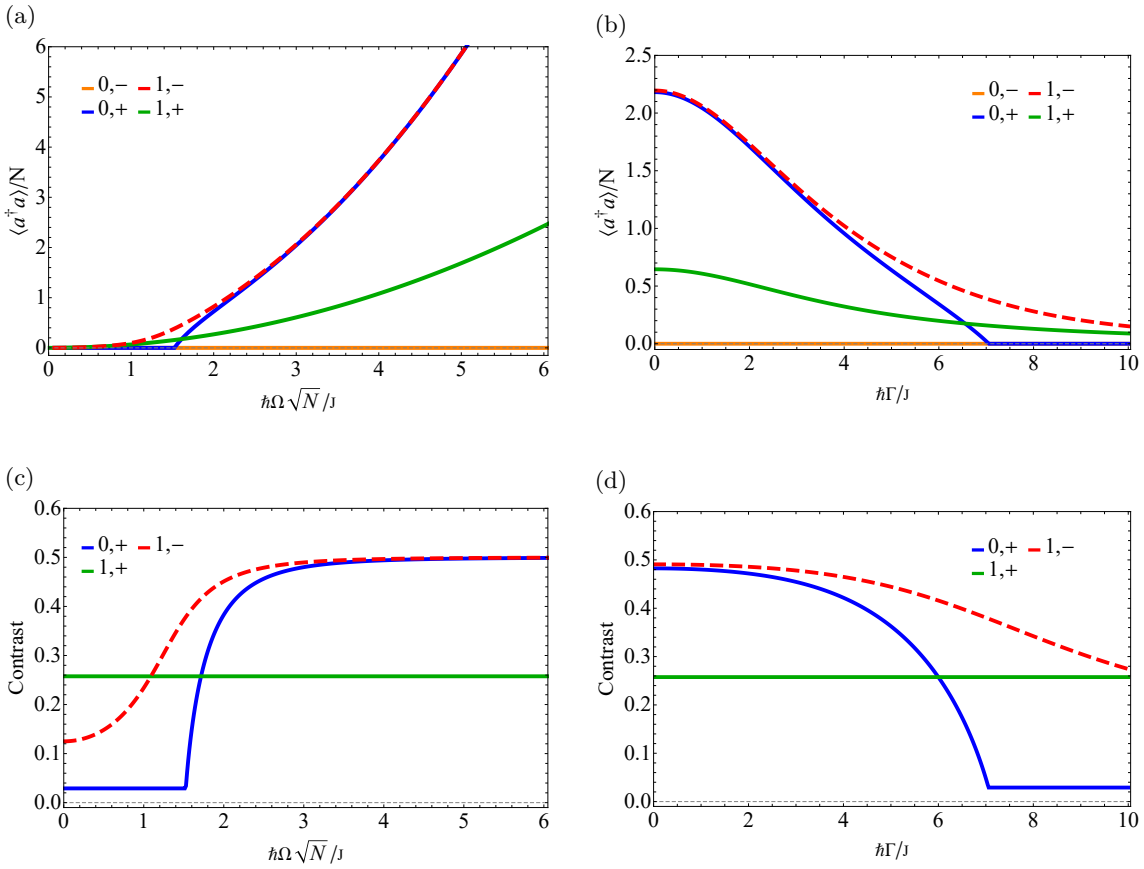

Figure 7.5: Results of the zero temperature mean-field approach. (a) and (c) show the dependence of the scaled photon number $\langle a^\dagger a\rangle/N$ and of the contrast on the scaled coupling strength $\Omega\sqrt{N}$ for $N = 2$ and $L = 4$. The parameters are $\hbar\delta/J = 2$, $U/J = 2$ and $\hbar\Gamma/J = 1$. (b) and (d) show the dependence of the scaled photon number $\langle a^\dagger a\rangle/N$ and of the contrast on the dissipation strength Γ for $N = 2$ and $L = 4$. The parameters are $\hbar\delta/J = 2$, $U/J = 2$ and $\hbar\Omega\sqrt{N}/J = 3$.

[1]Note that this is also true for the particle hole symmetry present in the half-filled case. However, since this symmetry has not been implemented, it will not be discussed further.

The solution in the symmetry sector $(0,+)$ is essentially the same as the solution obtained with open boundary conditions, since the lowest energy regarding all symmetry sectors is in the $(0,+)$ sector. There is a small shift in the transition threshold because of the influence of the different boundary conditions. Going to larger system sizes should reduce this effect. Completely new are now the solutions in the symmetry sectors $(0,-)$, $(1,-)$ and $(1,+)$. Since the Hamiltonian vanishes in the $(0,-)$ symmetry sector, it is clear why we do not see any dynamics in the photon number. Therefore, we will neglect this sector in the discussion of the other observables. The solutions in the sectors $(1,-)$ and $(1,+)$ show a very different behavior compared to the solutions we have seen so far for the interacting model. In contrast to a sharp phase transition, we see a smooth and continuous increase of the cavity occupation by increasing coupling strength, which is similar to the behavior seen in the non-interacting model in the $\pi/2$ symmetry sector. If we look at the contrast depicted in Fig. 7.5c and 7.5d, we see again that the states in the sectors $(0,+)$ and $(1,-)$ approach a total population imbalance in the self-organized phase whereas the contrast in the symmetry sector $(1,+)$ is just constant across both phases.

Comparing this to the results of the mean-field solutions including fluctuations shown in Fig. 7.6, we see the same differences across the symmetry sectors which we already observed in the case of open boundary conditions. The increase of the effective temperature in the self-organized phase (see Fig. 7.6e) leads to a suppressed photon number (see Fig. 7.6a) and a suppressed contrast (see Fig. 7.6c). The latter means that the atomic state is not just given by a pure state with perfect population imbalance. It includes also states with defects in the population imbalance. In contrast to the situation for open boundary conditions, we do not see a jump at the phase transition in Fig. 7.6a, Fig. 7.6c and Fig. 7.6d. Regarding the solution in the symmetry sector $(1,+)$, we see that the temperature stays also constant across the phase transition. However, in the strong dissipation regime, the contrast (see Fig. 7.6d) and the temperature (see Fig. 7.6f) slightly change and are not constant anymore.

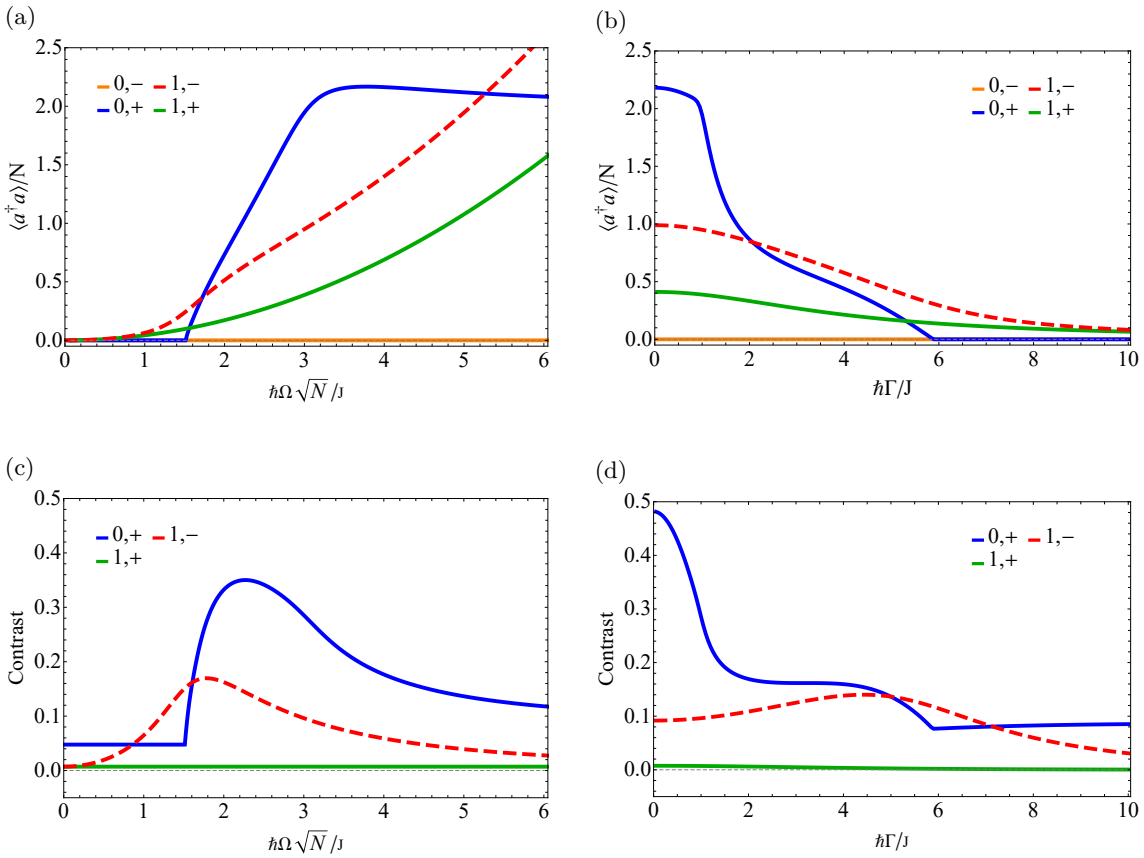

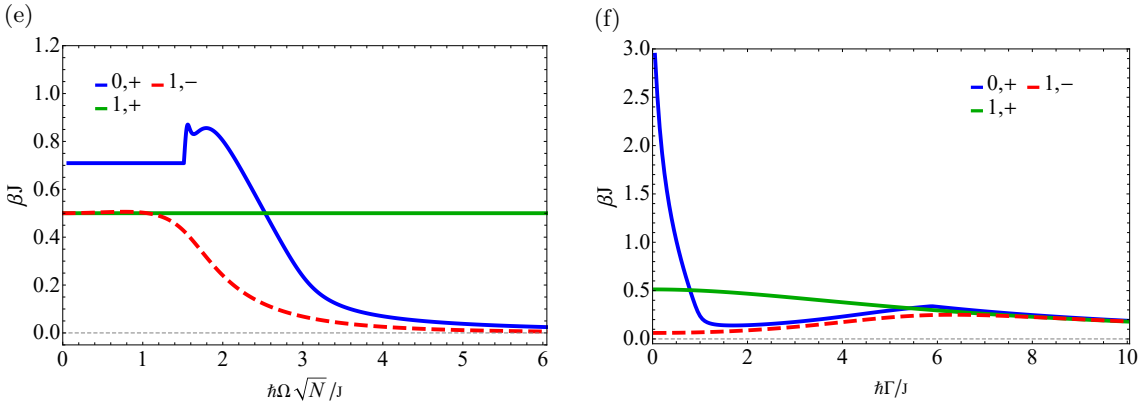

Figure 7.6: Results of the finite temperature many-body adiabatic elimination approach. (a), (c) and (e) show the dependence of the scaled photon number $\langle a^\dagger a\rangle/N$, of the contrast and of the inverse temperature β on the scaled coupling strength $\Omega\sqrt{N}$ for $N = 2$ and $L = 4$. The parameters are $\hbar\delta/J = 2$, $U/J = 2$ and $\hbar\Gamma/J = 1$. (b), (d) and (f) show the dependence of the scaled photon number $\langle a^\dagger a\rangle/N$, of the contrast and of the inverse temperature β on the dissipation strength Γ for $N = 2$ and $L = 4$. The parameters are $\hbar\delta/J = 2$, $U/J = 2$ and $\hbar\Omega\sqrt{N}/J = 3$.

In the half-filled case, i.e. $N = 4$ and $L = 4$, we can see the solutions of the zero temperature mean-field approach in Fig. 7.7. Here, we also discuss the $(0, -)$ symmetry sector since this time dynamics are present in this sector. Comparing the results to the ones for open-boundary conditions (see Fig. 7.3), we observe no jump at the phase transition. In comparison to the results of the zero temperature mean-field solutions for periodic boundary conditions for quarter-filling shown in Fig. 7.5, we now observe a sharp phase transition in the symmetry sectors $(1, -)$ and $(1, +)$ and a smoother increase of the photon number in the sector $(0, +)$. Moreover, the solutions of the symmetry sectors $(1, -)$ and $(1, +)$ are matching. If we further look at the contrast depicted in figure 7.7c and 7.7d, only the solution in the symmetry sector $(0, +)$ reaches a total population imbalance.

Fig. 7.8 shows how the behavior for half-filling changes after including fluctuations. First of all, there is no jump at the phase transition in contrast to the prominent one for open boundary conditions shown in Fig. 7.4. Secondly, the fluctuations lead to a sharp increase of the photon number in the symmetry sector $(0, +)$ in contrast to the zero temperature mean-field solution for the same filling. Furthermore, this solution has some small wiggles in the curves of all observables, which we do not saw previously in any situation. It might be that these are finite size effects. The solutions of the sectors $(1, -)$ and $(1, +)$ are again matching like the ones obtained in the zero temperature mean-field approach. The solution in the sector $(0, -)$ seems to fluctuate in some regions, especially in the inverse temperature in Fig. 7.8f. Increasing the accuracy in the calculation of this solution has not removed these fluctuations. These might be finite size effects. Again, the photon number and the contrast are much below the ones from the zero temperature mean-field solutions in all of the four symmetry sectors. Apart from the solutions in the symmetry sectors $(1, -)$ and $(1, +)$ for a fixed dissipation strength Γ, the transition thresholds compared to the ones from the zero temperature mean-field solutions deviate a bit.

In conclusion, likewise to the case of open boundary conditions we have seen that fluctuations play a crucial role for the steady state solutions in our system. Moreover, we investigated the influence of strong symmetries onto the nature of these steady states. In each of the resulting symmetry sectors we found a steady state solution and studied the resulting phase transitions into a self-organized phase. The results were very different regarding the transition threshold and the general behavior.

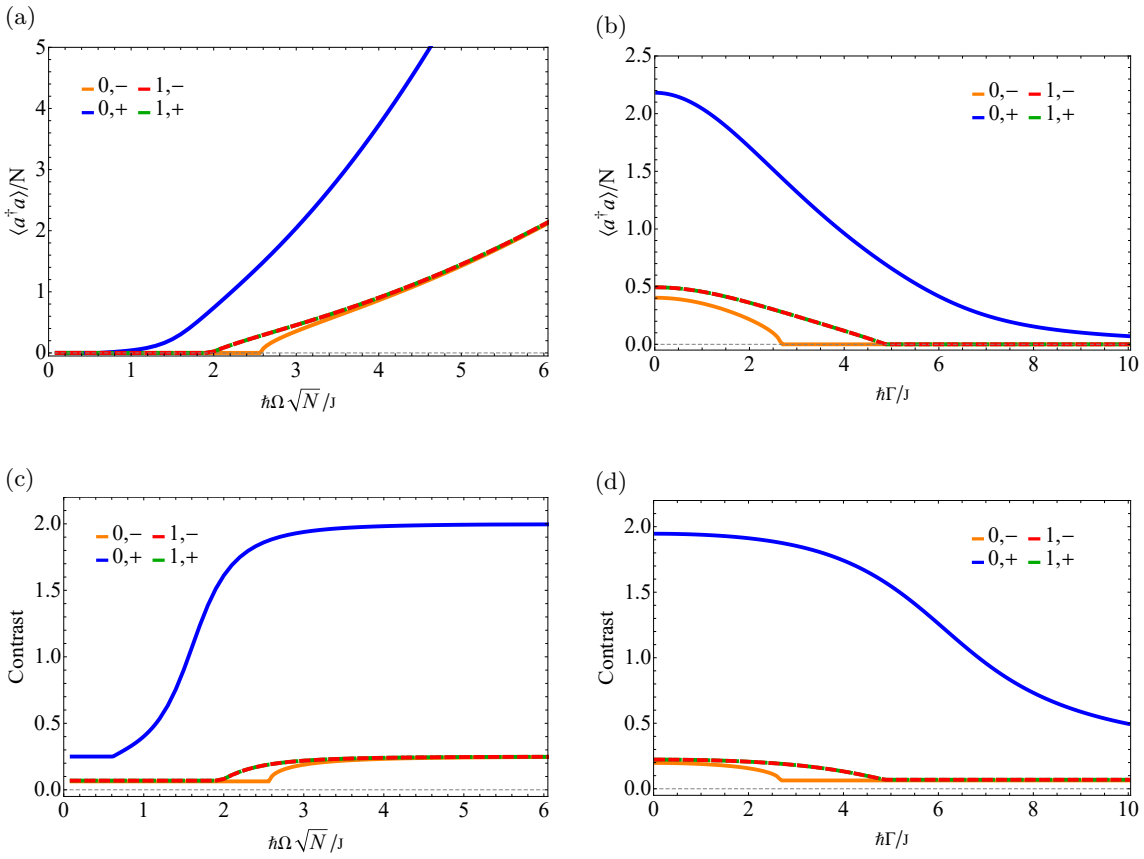

Figure 7.7: Results of the zero temperature mean-field approach. (a) and (c) show the dependence of the scaled photon number $\langle a^\dagger a\rangle/N$ and of the contrast on the scaled coupling strength $\Omega\sqrt{N}$ for $N = 4$ and $L = 4$. The parameters are $\hbar\delta/J = 2$, $U/J = 2$ and $\hbar\Gamma/J = 1$. (b) and (d) show the dependence of the scaled photon number $\langle a^\dagger a\rangle/N$ and of the contrast on the dissipation strength Γ for $N = 4$ and $L = 4$. The parameters are $\hbar\delta/J = 2$, $U/J = 2$ and $\hbar\Omega\sqrt{N}/J = 3$.

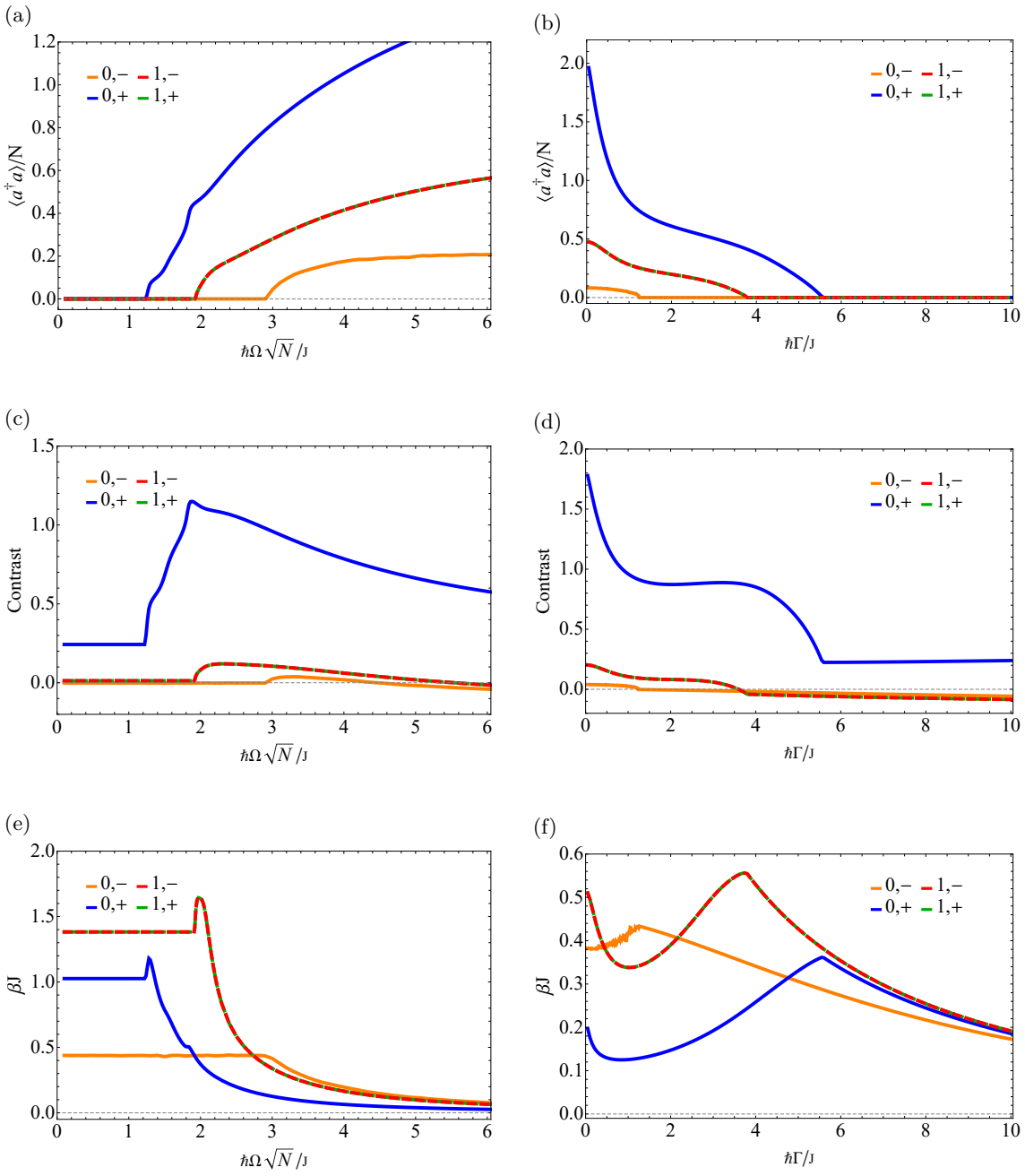

Figure 7.8: Results of the finite temperature many-body adiabatic elimination approach. (a), (c) and (e) show the dependence of the scaled photon number $\langle a^\dagger a\rangle/N$, of the contrast and of the inverse temperature β on the scaled coupling strength $\Omega\sqrt{N}$ for $N = 4$ and $L = 4$. The parameters are $\hbar\delta/J = 2$, $U/J = 2$ and $\hbar\Gamma/J = 1$. (b), (d) and (f) show the dependence of the scaled photon number $\langle a^\dagger a\rangle/N$, of the contrast and of the inverse temperature β on the dissipation strength Γ for $N = 4$ and $L = 4$. The parameters are $\hbar\delta/J = 2$, $U/J = 2$ and $\hbar\Omega\sqrt{N}/J = 3$.

8 Conclusion

In this thesis, we investigated the self-organization transition present in our system consisting of fermionic atoms which are confined to an optical lattice and which are globally coupled to the field of a dissipative optical cavity. Using a newly developed many-body adiabatic elimination method [11, 13], we captured the dissipative nature of the quantum light field as well as the global coupling to the cavity mode beyond the mean-field decoupling. Within this approach, we described the atomic part of the density matrix of the interacting model by a thermal state. In order to justify the applicability of this ansatz, we checked the non-integrability of the ionic Hubbard model. For this, we discussed the different symmetries which are present in the system, i.e. particle number conservation, SU(2) symmetry, translation symmetry and refelction symmery. By analyzing the level statistics in the different symmetry sectors, we found a GOE distribution in the quarter-filled case for a broad range of parameters showing the non-integrability of the model. Because of an additional symmetry in the half-filled case, i.e. a particle hole symmetry, we did not saw a clear GOE behavior in the level statistics. In this case, we showed that the distribution agrees well with the one of a GOE where a further splitting into two symmetry blocks is still possible, which suggested again that the ionic Hubbard model in non-integrable. To support this even more, we changed the interaction term so that the interaction strength is different on even and odd sites of the chain. This breaks the particle hole symmetry while the others remain valid. Here we obtained again a GOE distribution. We concluded that the ionic Hubbard model in non-integrable.

We proceeded by first investigating the non-interacting model. This was done by calculating the steady state solutions within the many-body elimination method by solving for every entry of the atomic density matrix. For this, we introduced the concept of symmetries in open quantum systems and found a strong symmetry for our non-interacting model. In the presence of this symmetry, we obtained multiple steady state solutions in the different symmetry sectors. By looking at the cavity occupation as a function of the coupling strength, we observed the self-organization transition. This transition changed for the different steady state solutions regarding the transition threshold. Some solutions were completely different in their nature meaning that they showed a smooth increase of the cavity occupation.

In the interacting model, we focused on the differences between the zero temperature mean-field solutions and the solutions calculated by including the fluctuations of the mean-field decoupling within the many-body adiabatic elimination. We observed that fluctuations really change the behavior of the phase transition. We saw this in the suppressed photon number and also in the suppressed density-density correlations. Without fluctuations the atomic state in the mean-field treatment approaches a total population imbalance where no defects are present. Fluctuations lead to a finite temperature and a mixed atomic state in the self-organized phase meaning that states without a total population imbalance do also contribute to the state. Furthermore, we studied the influence of strong symmetries in this interacting model for periodic boundary conditions, where the strong symmetries were given by a translation symmetry and a reflection symmetry. Similar to the non-interacting model, the transition threshold of the dissipative phase transition changed for the different sectors. Moreover, some solutions did not showed a sharp onset of the cavity occupation at all. Since the thermal ansatz of the atomic density matrix is only valid for a non-integrable model which corresponds to the regime above the transition, one has to further investigate how one could appropriately describe the regime below the transition. Another objective for the future would be to investigate more parameter regimes and to improve the numerical implementations in order to be able to go to larger system sizes.

References

[1] Iulia M Georgescu, Sahel Ashhab, and Franco Nori. Quantum simulation. *Reviews of Modern Physics*, 86(1):153, 2014.

[2] Kristian Baumann, Christine Guerlin, Ferdinand Brennecke, and Tilman Esslinger. Dicke quantum phase transition with a superfluid gas in an optical cavity. *nature*, 464(7293):1301–1306, 2010.

[3] Renate Landig, Lorenz Hruby, Nishant Dogra, Manuele Landini, Rafael Mottl, Tobias Donner, and Tilman Esslinger. Quantum phases from competing short-and long-range interactions in an optical lattice. *Nature*, 532(7600):476–479, 2016.

[4] Xiaotian Zhang, Yu Chen, Zemao Wu, Juan Wang, Jijie Fan, Shujin Deng, and Haibin Wu. Observation of a superradiant quantum phase transition in an intracavity degenerate fermi gas. *Science*, 373(6561):1359–1362, 2021.

[5] Heinz-Peter Breuer, Francesco Petruccione, et al. *The theory of open quantum systems*. Oxford University Press on Demand, 2002.

[6] Christoph Maschler, Igor B Mekhov, and Helmut Ritsch. Ultracold atoms in optical lattices generated by quantized light fields. *The European Physical Journal D*, 46(3):545–560, 2008.

[7] Helmut Ritsch, Peter Domokos, Ferdinand Brennecke, and Tilman Esslinger. Cold atoms in cavity-generated dynamical optical potentials. *Reviews of Modern Physics*, 85(2):553, 2013.

[8] Farokh Mivehvar, Francesco Piazza, Tobias Donner, and Helmut Ritsch. Cavity qed with quantum gases: New paradigms in many-body physics. *arXiv preprint arXiv:2102.04473*, 2021.

[9] Catalin-Mihai Halati, Ameneh Sheikhan, Helmut Ritsch, and Corinna Kollath. Numerically exact treatment of many-body self-organization in a cavity. *Physical Review Letters*, 125(9):093604, 2020.

[10] Catalin-Mihai Halati, Ameneh Sheikhan, and Corinna Kollath. Theoretical methods to treat a single dissipative bosonic mode coupled globally to an interacting many-body system. *Physical Review Research*, 2(4):043255, 2020.

[11] Alla V Bezvershenko, Catalin-Mihai Halati, Ameneh Sheikhan, Corinna Kollath, and Achim Rosch. Dicke transition in open many-body systems determined by fluctuation effects. *Physical review letters*, 127(17):173606, 2021.

[12] Catalin-Mihai Halati, Ameneh Sheikhan, and Corinna Kollath. Breaking strong symmetries in dissipative quantum systems: the (non-) interacting bosonic chain coupled to a cavity. *arXiv preprint arXiv:2102.02537*, 2021.

[13] Cătălin-Mihai Halaţi. External control of many-body quantum systems. 2021.

[14] Bruno Sciolla, Dario Poletti, and Corinna Kollath. Two-time correlations probing the dynamics of dissipative many-body quantum systems: Aging and fast relaxation. *Physical review letters*, 114(17):170401, 2015.

[15] Corinna Kollath, Guillaume Roux, Giulio Biroli, and Andreas M Läuchli. Statistical properties of the spectrum of the extended bose–hubbard model. *Journal of Statistical Mechanics: Theory and Experiment*, 2010(08):P08011, 2010.

[16] Abolfath Hosseinzadeh and Seyed Akbar Jafari. Quantum integrability of 1d ionic hubbard model. *Annalen der Physik*, 532(3):1900601, 2020.

[17] Elliott H. Lieb and F. Y. Wu. Absence of mott transition in an exact solution of the short-range, one-band model in one dimension. *Phys. Rev. Lett.*, 20:1445–1448, Jun 1968.

[18] Didier Poilblanc, Timothy Ziman, Jean Bellissard, Frederic Mila, and Gilles Montambaux. Poisson vs. goe statistics in integrable and non-integrable quantum hamiltonians. *EPL (Europhysics Letters)*, 22(7):537, 1993.

[19] Y. Y. Atas, E. Bogomolny, O. Giraud, and G. Roux. Distribution of the ratio of consecutive level spacings in random matrix ensembles. *Phys. Rev. Lett.*, 110:084101, Feb 2013.

[20] Olivier Giraud, Nicolas Macé, Eric Vernier, and Fabien Alet. Probing symmetries of quantum many-body systems through gap ratio statistics. *arXiv preprint arXiv:2008.11173*, 2020.

[21] Victor V Albert and Liang Jiang. Symmetries and conserved quantities in lindblad master equations. *Physical Review A*, 89(2):022118, 2014.

[22] Berislav Buča and Tomaž Prosen. A note on symmetry reductions of the lindblad equation: transport in constrained open spin chains. *New Journal of Physics*, 14(7):073007, 2012.

[23] Catalin-Mihai Halati, Ameneh Sheikhan, and Corinna Kollath. Cavity-induced artificial gauge field in a bose-hubbard ladder. *Physical Review A*, 96(6):063621, 2017.